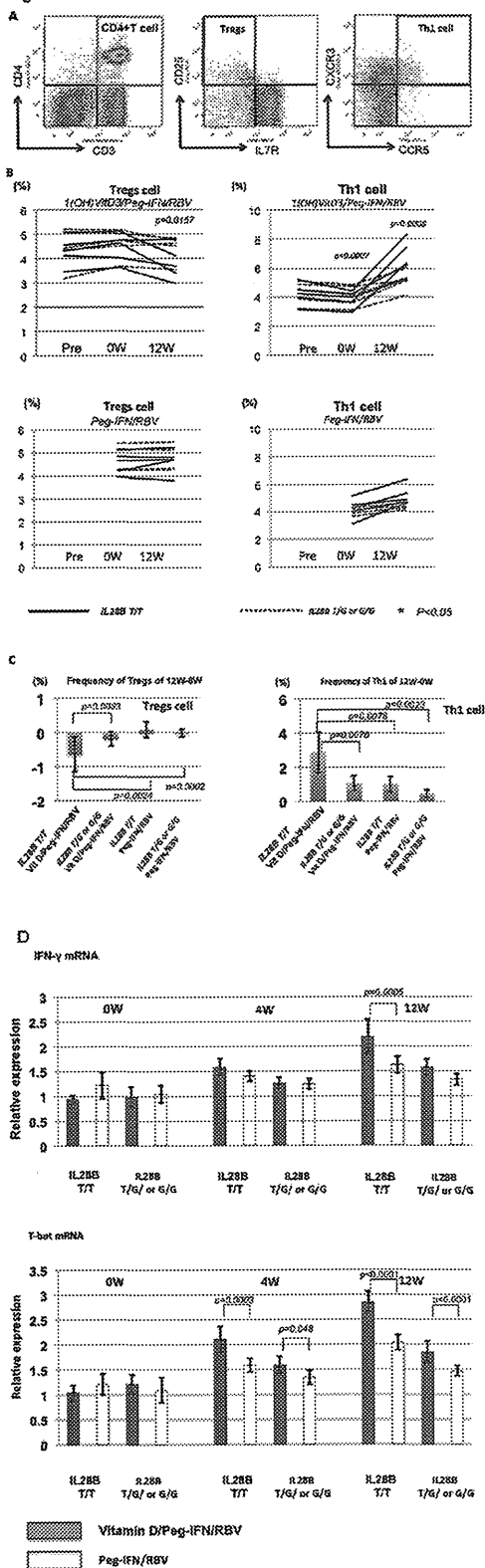Figure 5. Comparison of Th1 and Tregs between 1(OH) vitamin D3/Peg-IFN/RBV and Peg-IFN/RBV. Representative dot plots of CD3⁺CD4⁺CD25⁺IL7R⁻ (Tregs) and CD3⁺CD4⁺CXCR3⁺CCR5⁺ (Th1 cells) are shown. (A) Frequencies of Th1 and Tregs among the 4 groups (IL28B T/T vitamin D3/Peg-IFN/RBV, IL28B T/G or G/G vitamin D3/Peg-IFN/RBV, IL28B T/T Peg-IFN/RBV, and IL28B T/G or G/G Peg-IFN/RBV) are shown. (B) Comparison of the T-bet and IFN-γ mRNA expression between subjects treated with vitamin D3/Peg-IFN/RBV therapy and those treated with Peg-IFN/RBV therapy. Each group included 5 patients. Total mRNA was extracted from isolated CD4⁺ T cells. The relative expression levels are shown in bar graphs. The statistical analysis was carried out by independent student t-test.
doi:10.1371/journal.pone.0063672.g005

were previously treated with IFN-based therapy and failed to achieve SVR. Another 29 patients were treatment naïve. Case match control subjects treated with Peg-IFN/RBV therapy were enrolled in this study (Fig. 1) (Table 1). All of the enrolled patients had over 5 log copies/ml HCV-RNA and genotype 1b HCV RNA. Thirteen patients had the hetero/minor *IL28B* allele (T/G) (rs8099917) that was reported to be a marker of patients difficult-to-treat with Peg-IFN/RBV therapy [29]. Twenty-nine patients had the major homo *IL28B* allele (T/T) that was reported to be favorable for achieving SVR [29]. Therefore, we compared the viral dynamics between subjects treated with the 1(OH) vitamin D3/Peg-IFN/RBV and subjects receiving the Peg-IFN/RBV with the same IL28B polymorphism (Fig. 2A and B). The titers of HCV-RNA in the *IL28B* (T/T)-HCV patients treated with 1(OH) vitamin D3/Peg-IFN/RBV therapy were significantly lower than those treated with Peg-IFN/RBV at 4 weeks after the start of Peg-IFN/RBV therapy ($p<0.01$). The rate of early virological response in the *IL28B* (T/T) patients treated with 1(OH) vitamin D3/Peg-IFN/RBV was significantly higher than that in those treated with Peg-IFN/RBV alone (Fig. 2C). None of the patients showed side effects from 1(OH) vitamin D3 administration such as hypercalcemia or renal dysfunction, etc. The rate of the sustained virological response (SVR) in the overall patients treated with 1(OH) vitamin D3/Peg-IFN/RBV was 59.45% (45.24% in the overall patients treated with Peg-IFN/RBV) ($p = 0.2059$) The rate of SVR in the *IL28B* (T/T) patients treated with 1(OH) vitamin D3/Peg-IFN/RBV was 73.07% (55.17% in *IL28B* (T/T) patients treated with Peg-IFN/RBV) ($p = 0.1657$). However, this study was conducted to analyze the immunological response during the early phase of Peg-IFN/RBV. The sample size might not be large enough to analyze the SVR rate.

Biological Effect of 1(OH) Vitamin D3 Treatment during Peg-IFN/RBV Therapy

The biochemical and hematological analysis was carried out at 4 weeks before the start of Peg-IFN/RBV therapy and at the start of Peg-IFN/RBV therapy. Of those data, only the absolute counts of white blood cells were significantly decreased after 4 weeks-1(OH) vitamin D3-treatment (p<0.05) (Fig. 3). The titers of HCV-RNA were not significantly changed after the 4-week administration of 1(OH) vitamin D3 without Peg-IFN/RBV therapy. Therefore, we examined the immunological effects of 1(OH) vitamin D3. At first, we quantitated 10 cytokines (IL4, IL6, IL10, IL12, IL17, IFN-γ, IP-10, MCP-1, RANTES, TNF-α) in the peripheral blood samples during 1(OH) vitamin D3/Peg-IFN/RBV therapy using multiple beads suspension array (Fig. 4A and Fig. S1). Among the *IL28B* T/T polymorphism patients, the amounts of IL4, IP-10 and MCP1 in the peripheral blood serum were significantly reduced after 4-week-1(OH) vitamin D3-treatment. On the other hand, the amounts of IL6, RANTES and TNF-α in the serum were significantly increased after 4-week 1(OH) vitamin D3 treatment. In the *IL28B* T/G or G/G

— 76 —

A

B
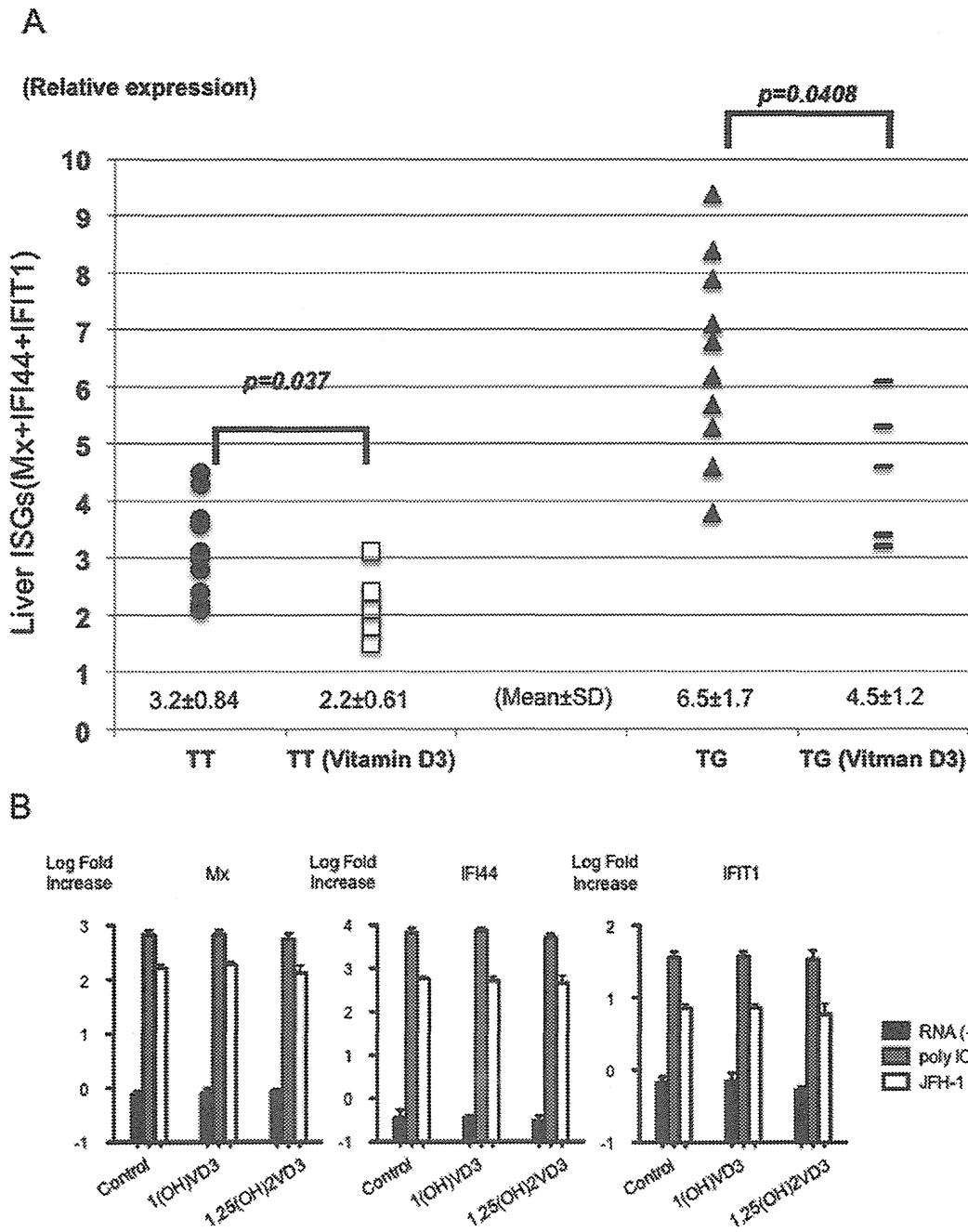
Figure 6. The effect of vitamin D3 on the expression of ISGs mRNA in the liver. The relative amount of target mRNA was obtained by using a comparative threshold cycle (CT) method. The expression levels of Mx, IFI44 or IFIT1 mRNA in an *IL28B T/T* patient treated without 1(OH) vitamin D3 are represented as 1.0 and the relative amounts of target mRNA in the other patients were calculated by the comparative Ct method [42]. Therefore, the standard amount of 3 ISGs (Mx, IFI44 and IFIT1) is 3. The relative amounts of the 3 kinds of ISGs were added and shown in the graph (A). Black circles indicate the data from IL28B (T/T) subjects treated without 1(OH) vitamin D3. White boxes indicate the data from IL28B (T/T) subjects treated with 1(OH) vitamin D3. Black triangles indicate the data from IL28B (T/G or G/G) subjects treated without 1(OH) vitamin D3. Black lines indicate the data from the subjects treated with 1(OH) vitamin D3 (A). The effect of vitamin D3 on the expression of ISGs mRNA in the hepatocyte cell culture are shown (B). Huh-7 cells were treated with ethanol (control), 1(OH) vitamin D3 (1.0 μM) or 1,25(OH)$_2$ vitamin D3 (1.0 μM) after transfection of poly IC (Sigma-Aldrich, St. Louis, MO) or in vitro transcribed JFH-1 full-length RNA. Cells were harvested 30 h after transfection, and the expression levels of Mx, IFI44 and IFIT1 mRNA were assessed by real-time PCR using TaqMan Gene Expression Master Mix (Applied Biosystems, Carlsbad, CA) and gene-specific primer and probe sets (TaqMan Gene Expression Assay; Applied Biosystems) in accordance with the manufacturer's instructions. The expression levels of genes with or without vitamin D3 treatment were expressed by log fold increase of untreated Huh-7 cells.
doi:10.1371/journal.pone.0063672.g006

– 77 –

polymorphism patients, the amount of RANTES in the serum was significantly increased after 4-week 1(OH) vitamin D3-treatment. The amounts of IL4, IFN-γ, IP-10, MCP-1 in the serum were significantly decreased after 4-week 1(OH) vitamin D3-treatment. The administration of 1 (OH) vitamin D3 could reduce the high IP-10 status that is reported to be difficult-to-treat. Then, we compared the amounts of 10 cytokines between 1(OH) vitamin D3/Peg-IFN/RBV group and Peg-IFN/RBV group at 0 week and 12 weeks after the Peg-IFN/RBV treatment. The amounts of cytokines in the patients treated with 1(OH) vitamin D3/Peg-IFN/RBV at 0 week were affected by 4 weeks 1(OH) vitamin D3 pre-treatment. The amounts of IP-10 in the patients treated with 4 weeks-1(OH) vitamin D3 were significantly lower than those in the group treated without 1(OH) vitamin D3. However, the amounts of IFN-gamma and RANTES in the *IL28B* TT patients treated with 1(OH) vitamin D3/Peg-IFN/RBV were significantly higher than those in the *IL28B* TT patients treated with Peg-IFN/RBV without 1(OH) vitamin D3 at 12 weeks after the start of Peg-IFN/RBV treatment (Fig. 4B). In addition to the absolute amounts of several cytokines, the changes in the amounts after the 12 weeks Peg-IFN/RBV treatment were analyzed (Fig. 4B and Fig. S2). Changes in the amounts of IL4, IL-12, IFN-gamma and RANTES during the 12 weeks-treatment of Peg-IFN/RBV were significantly different between the 1(OH) vitamin D3/Peg-IFN/RBV group and Peg-IFN/RBV group (p<0.05) (Fig. 4B and Fig. S2).

The Biological Effects of 1(OH)vitamin D3 and 1,25(OH)$_2$ Vitamin D3 on the Production of Cytokines from PBMCs

Then, we examined whether the administration of 1(OH) vitamin D3 could affect the production of various kinds of cytokines from PBMCs. We used trans-well systems to analyze the effects of hepatocytes with various kinds of enzymes that affect the metabolism of 1(OH) vitamin D3 (Fig. 4C). We used a ng/ml order of calcitriol(1,25(OH)$_2$ vitamin D3) as the active form of vitamin D3 and a μg/ml order of 1(OH) vitamin D3 as the pre-active form of vitamin D3 with or without IFN-α (0.025 ng/ml). The amounts of IL4, IL6, IFN-γ, IP-10 and TNF-α were significantly decreased by the active and pre-active form of vitamin D3 without IFN-α (Fig. 4D). Among them, the amount of IP-10 was dose-dependently decreased by 1(OH)vitamin D3 and 1,25(OH)$_2$vitamin D3 without IFN-α. On the other hand, the amount of RANTES was dose-dependently increased by 1(OH)-vitamin D3 and 1,25 (OH)$_2$ vitamin D3 with or without IFN-α. The amounts of IL10 and IFN-γ were significantly increased by 1(OH)vitamin D3 and 1,25(OH)$_2$vitamin D3 with IFN-α (Fig. 4D). These data indicated that 1(OH)vitamin D3 and 1,25(OH)$_2$vitamin D3 could modulate the immunological status of PBMCs, especially the down-regulation of IP-10 production.

Comparison of the Frequency of Th1 and Tregs between 1(OH) Vitamin D3/Peg-IFN/RBV and Peg-IFN/RBV

Sequential analyses of CD3$^+$CD4$^+$CXCR3$^+$CCR5$^+$(Th1 cells) and CD3$^+$CD4$^+$CD25$^+$CD127$^-$ (Tregs) were carried out during 1(OH) vitamin D3/Peg-IFN/RBV or Peg-IFN/RBV treatment. Representative dot plots indicating Th1 and Tregs are shown (Fig. 5A). The subsets of these cells could be clearly recognized by flow cytometry. Four-week treatment of 1(OH) vitamin D3 could significantly decrease the frequency of Th1 cells but not Tregs (p<0.05) (Fig. 5B). However, the frequency of Th1 cells was rapidly increased after the start of Peg-IFN/RBV therapy, especially in the *IL28B* T/T subjects treated with 1(OH) vitamin D3/Peg-IFN/RBV therapy (Fig. 5B and C). The frequency of Th1 cells in the subjects treated with 1(OH) vitamin D3 was significantly higher than in those treated with Peg-IFN/RBV at 12

weeks after the Peg-IFN/RBV therapy, especially in the *IL28B* T/T patients (Fig. 5C). Moreover, the expression of IFN-γ and T-bet mRNA in the isolated CD4$^+$ cells of subjects treated with 1(OH) vitamin D3/Peg-IFN/RBV therapy was significantly higher than in those treated with Peg-IFN/RBV therapy at 4 weeks and 12 weeks after Peg-IFN/RBV therapy (Fig. 5D).

Changes in ISG mRNA Expression in Liver with 1(OH) Vitamin D3 Treatment

The administration of 1(OH) vitamin D3 could reduce various kinds of cytokines in the serum. Therefore, we carried out quantification of ISG mRNA in samples from liver biopsies (Fig. 6A). We selected the Mx, IFI44, IFIT1 genes among the various kinds of ISGs, since another group previously reported that these ISGs could clearly recognize patients as difficult-to treat or easy-to-treat with IFN-based therapy [30]. The expression level of ISGs in the *IL28B* TT polymorphism was significantly lower than in the *IL28B* TG or GG polymorphism. Moreover, the expression levels of liver ISGs in the CH-C patients receiving 4 week-administration of 1(OH) vitamin D3 were significantly lower than those in the CHC patients without administration of 1(OH) vitamin D3.

Direct Effect of Vitamin D on the Expression of ISGs in Hepatocyte without Immune Cells

We used Huh-7 cells with a JFH-1 system that mimicks the acute phase of ISG induction in HCV infection, since we wanted to determine whether 1 (OH) vitamin D3 and 1, 25 (OH)2 vitamin D3 could affect the ISG expression directly. Three representative ISGs (MxA, IFI44 and IFIT1) were analyzed by real-time PCR. JFH-1 replication could induce these ISGs in Huh-7 cells (Fig.6 B). We used 1(OH) vitamin D3 and 1,25(OH)$_2$ vitamin D3 to analyze the ISG expression after JFH-1 inoculation. These ISGs were not affected by 1(OH) vitamin D3, and 1, 25(OH)$_2$ vitamin D3 in vitro.

Discussion

Recently, it has been reported that supplementation of vitamin D3, a potent immunomodulator, could improve the HCV response to antiviral therapy [2,3,31]. We used 1(OH) vitamin D3, since hepatocytes have various kinds of enzymes to convert 1(OH) vitamin D3 to the active metabolite 1,25(OH)$_2$ vitamin D3. Therefore, we speculated that the administration of 1(OH) vitamin D3 could affect the liver adaptive immune cells since the local concentration of 1,25(OH)$_2$ vitamin D3 might be higher than the systemic concentration of this active metabolite. Another group reported that 25(OH) vitamin D3, but not vitamin D3 or 1,25(OH)$_2$ vitamin D3, could have direct-antiviral activity at the level of infectious virus assembly [7]. However, the antiviral activity of 25(OH) vitamin D3 is not so remarkable. Moreover, the system of HCV replication in that study did not include the immune cells that are important for the control of HCV replication [32–35].

In this study, we first reported that administration of 1(OH) vitamin D3 could affect the cytokine production from PBMCs and suppress the ISGs mRNA expression in the liver samples. Among the various kinds of cytokines, IP-10, which was reported to be an important biomarker for the treatment response, could be significantly decreased after 1(OH) vitamin D3 treatment in vivo [36,37]. It has been reported that a high amount of IP-10 is a promising biomarker for difficult-to-treat patients regardless of the *IL28B* polymorphism [36,37]. IP-10 can be produced from various kinds of immune cells including monocytes. In this study, we found

– 78 –

that calcitriol could reduce the production of IP-10 from PBMCs dose-dependently *in vitro*. In addition to the production of IP-10, the expression of ISG mRNA in the liver biopsy samples with 1(OH) vitamin D3 treatment was significantly lower than in those without 1(OH) vitamin D3 treatment regardless of the *IL28B* polymorphism. The excessive expression of ISG mRNA before the Peg-IFN/RBV therapy might induce a poor response to IFN administration [38,39]. In addition to these results, we confirmed that the amounts of IFN-gamma and RANTES induced by 12-weeks 1 (OH) vitamin D3/Peg-IFN/RBV treatment was significantly higher than those induced by 12 weeks Peg-IFN/RBV treatment without 1 (OH) vitamin D3. 1 (OH) vitamin D3 could suppress the basal levels of the immune response in the CH-C patients. However, the subsequent response of the adaptive immune system after the start of Peg-IFN/RBV treatment could have been augmented by 1(OH) vitamin D3. These data indicated that calcitriol might be able to stabilize the adaptive immune systems that were out of control in CH-C patients instead of inducing their activation. In this study, we could not detect a significantly higher rate of SVR in the 1(OH) vitamin D3/Peg-IFN/RBV group in comparison with those in the Peg-IFN/RBV group. However, the addition of 1(OH) vitamin D3 could improve the adaptive immune response. Therefore, the SVR rate in the 1(OH) vitamin D3/Peg-IFN/RBV group might have been significantly higher than in the Peg-IFN/RBV group, if the sample size had been large enough to analyze the SVR.

In addition to previous reports, our data indicated that calcitriol could affect the production of cytokines from PBMCs [25,40]. However, we could not exclude the possibility of affecting cytokines other than the 10 cytokines we analyzed in this study. Moreover, other groups reported that vitamin D3 might modulate the expression of TLRs and/or their signaling, which are important in the immunopathogenesis of hepatitis C virus persistent infection [6,14,41]. This study was not a randomized control trial and did not have a large number of patients, since it focused on the effect of 1,25 $(OH)_2$ Vitamin D3 on the immune cells. For this purpose, the number of included patients was sufficient for the analysis. Moreover, we are conducting a randomized control trial that includes a large number of chronic hepatitis C patients with sever fibrosis and low vitamin D3 concentrations (ongoing study) (UMIN000007400).

In conclusion, the active metabolite of vitamin D3, calcitriol, could improve the response to Peg-IFN/RBV therapy. Supplementation of 1(OH) vitamin D3 or 1,25$(OH)_2$ vitamin D3 should be reasonable for the conditioning of IFN-based treatment including Direct Acting Antiviral (DAA)/Peg-IFN/RBV, DAA/Peg-IFN, Peg-IFN/RBV and Peg-IFN monotherapy.

Supporting Information

Figure S1 Cytokine profiles in the *ex vivo* treated with 1(OH) vitamin D3/Peg-IFN/RBV. Sequential data of quantification of 7 cytokines (IL4, IL6, IL10, IL12, IL17, MCP-1 and TNF-α) during 1(OH) vitamin D3 pre-treatment (pre vs 0w), 1(OH) vitamin D3/Peg-IFN/RBV therapy are shown. Dotted lines indicate the data of each subject. Black lines indicate the averaged data. Error bars indicate standard deviation. The data from IL28B (T/T) subjects or IL28B (T/G or G/G) subjects are shown in the separate graphs.
(TIFF)

Figure S2 Comparison of the cytokine profiles between 1(OH) vitamin D3 plus SOC and SOC. Comparisons in the amounts of 7 cytokines (IL4, IL6, IL10, IL12, IL17, MCP-1 and TNF-α) between 1(OH) Vitamin D3/PEG-IFN/RBV group (VitD3+standard of care (SOC)) and Peg-IFN/RBV group (SOC) at 0 weeks and 12 weeks after the start of Peg-IFN/RBV treatment are shown. Analysis of the changes in the amounts of 7 cytokines (IL4, IL6, IL10, IL12, IL17, MCP-1 and TNF-α) during 12 weeks treatment of Peg-IFN/RBV is shown.
(TIFF)

Author Contributions

References

1. Alter MJ, Kruszon-Moran D, Nainan OV, McQuillan GM, Gao F, et al. (1999) The prevalence of hepatitis C virus infection in the United States, 1988 through 1994. N Engl J Med 341: 556–562.
2. Abu-Mouch S, Fireman Z, Jarchovsky J, Zeina AR, Assy N (2011) Vitamin D supplementation improves sustained virologic response in chronic hepatitis C (genotype 1)-naive patients. World J Gastroenterol 17: 5184–5190.
3. Bitetto D, Fabris C, Fornasiere E, Pipan C, Fumolo E, et al. (2011) Vitamin D supplementation improves response to antiviral treatment for recurrent hepatitis C. Transpl Int 24: 43–50.
4. Bitetto D, Fattovich G, Fabris C, Ceriani E, Falleti E, et al. (2011) Complementary role of vitamin D deficiency and the interleukin-28B rs12979860 C/T polymorphism in predicting antiviral response in chronic hepatitis C. Hepatology 53: 1118–1126.
5. Petta S, Ferraro D, Camma C, Cabibi D, Di Cristina A, et al. (2012) Vitamin D levels and IL28B polymorphisms are related to rapid virological response to standard of care in genotype 1 chronic hepatitis C. Antiviral therapy 17: 823–831.
6. Gal-Tanamy M, Bachmetov L, Ravid A, Koren R, Erman A, et al. (2011) Vitamin D: an innate antiviral agent suppressing hepatitis C virus in human hepatocytes. Hepatology 54: 1570–1579.
7. Matsumura T, Kato T, Sugiyama N, Tasaka-Fujita M, Murayama A, et al. (2012) 25-hydroxyvitamin D(3) suppresses hepatitis C virus production. Hepatology.
8. Haddad JG, Matsuoka LY, Hollis BW, Hu YZ, Wortsman J (1993) Human plasma transport of vitamin D after its endogenous synthesis. The Journal of clinical investigation 91: 2552–2555.
9. DeLuca HF (1977) Regulation of vitamin D metabolism in the kidney. Advances in experimental medicine and biology 81: 195–209.
10. Deluca HF (1977) Vitamin D metabolism. Clinical endocrinology 7 Suppl: 1s–17s.
11. DeLuca HF (1977) Vitamin D endocrine system. Advances in clinical chemistry 19: 125–174.
12. Edfeldt K, Liu PT, Chun R, Fabri M, Schenk M, et al. (2010) T-cell cytokines differentially control human monocyte antimicrobial responses by regulating vitamin D metabolism. Proc Natl Acad Sci U S A 107: 22593–22598.
13. Bartosik-Psujek H, Tabarkiewicz J, Pocinska K, Stelmasiak Z, Rolinski J (2010) Immunomodulatory effects of vitamin D on monocyte-derived dendritic cells in multiple sclerosis. Mult Scler 16: 1513–1516.
14. Du T, Zhou ZG, You S, Lin J, Yang L, et al. (2009) Regulation by 1, 25-dihydroxy-vitamin D3 on altered TLRs expression and response to ligands of monocyte from autoimmune diabetes. Clin Chim Acta 402: 133–138.
15. Stio M, Treves C, Celli A, Tarantino O, d'Albasio G, et al. (2002) Synergistic inhibitory effect of cyclosporin A and vitamin D derivatives on T-lymphocyte proliferation in active ulcerative colitis. Am J Gastroenterol 97: 679–689.
16. Takahashi K, Nakayama Y, Horiuchi H, Ohta T, Komoriya K, et al. (2002) Human neutrophils express messenger RNA of vitamin D receptor and respond to 1alpha,25-dihydroxyvitamin D3. Immunopharmacology and immunotoxicology 24: 335–347.
17. Provvedini DM, Tsoukas CD, Deftos LJ, Manolagas SC (1983) 1,25-dihydroxyvitamin D3 receptors in human leukocytes. Science 221: 1181–1183.
18. Xu H, Soruri A, Gieseler RK, Peters JH (1993) 1,25-Dihydroxyvitamin D3 exerts opposing effects to IL-4 on MHC class-II antigen expression, accessory

– 79 –

activity, and phagocytosis of human monocytes. Scandinavian journal of immunology 38: 535–540.

19. Piemonti L, Monti P, Sironi M, Fraticelli P, Leone BE, et al. (2000) Vitamin D3 affects differentiation, maturation, and function of human monocyte-derived dendritic cells. Journal of immunology 164: 4443–4451.

20. Hewison M, Freeman L, Hughes SV, Evans KN, Bland R, et al. (2003) Differential regulation of vitamin D receptor and its ligand in human monocyte-derived dendritic cells. J Immunol 170: 5382–5390.

21. Khoo AL, Joosten I, Michels M, Woestenenk R, Preijers F, et al. (2011) 1,25-Dihydroxyvitamin D3 inhibits proliferation but not the suppressive function of regulatory T cells in the absence of antigen-presenting cells. Immunology 134: 459–468.

22. Khoo AL, Chai LY, Koenen HJ, Sweep FC, Joosten I, et al. (2011) Regulation of cytokine responses by seasonality of vitamin D status in healthy individuals. Clin Exp Immunol 164: 72–79.

23. Unger WW, Laban S, Kleijwegt FS, van der Slik AR, Roep BO (2009) Induction of Treg by monocyte-derived DC modulated by vitamin D3 or dexamethasone: differential role for PD-L1. Eur J Immunol 39: 3147–3159.

24. Mariani E, Ravaglia G, Forti P, Meneghetti A, Tarozzi A, et al. (1999) Vitamin D, thyroid hormones and muscle mass influence natural killer (NK) innate immunity in healthy nonagenarians and centenarians. Clin Exp Immunol 116: 19–27.

25. Mayne CG, Spanier JA, Relland LM, Williams CB, Hayes CE (2011) 1,25-Dihydroxyvitamin D3 acts directly on the T lymphocyte vitamin D receptor to inhibit experimental autoimmune encephalomyelitis. Eur J Immunol 41: 822–832.

26. Barchetta I, Carotti S, Labbadia G, Gentilucci UV, Muda AO, et al. (2012) Liver vitamin D receptor, CYP2R1, and CYP27A1 expression: relationship with liver histology and vitamin D3 levels in patients with nonalcoholic steatohepatitis or hepatitis C virus. Hepatology 56: 2180–2187.

27. Abu-Mouch SM, Fireman Z, Jarchovsky J, Assy N (2009) The Beneficial Effect of Vitamin D with Combined Peg Interferon and Ribavirin for Chronic Hcv Infection. Hepatology 50: 12A–13A.

28. Kakazu E, Ueno Y, Kondo Y, Fukushima K, Shiina M, et al. (2009) Branched chain amino acids enhance the maturation and function of myeloid dendritic cells ex vivo in patients with advanced cirrhosis. Hepatology 50: 1936–1945.

29. Tanaka Y, Nishida N, Sugiyama M, Kurosaki M, Matsuura K, et al. (2009) Genome-wide association of IL28B with response to pegylated interferon-alpha and ribavirin therapy for chronic hepatitis C. Nat Genet 41: 1105–1109.

30. Honda M, Sakai A, Yamashita T, Nakamoto Y, Mizukoshi E, et al. (2010) Hepatic ISG expression is associated with genetic variation in interleukin 28B and the outcome of IFN therapy for chronic hepatitis C. Gastroenterology 139: 499–509.

31. Nimer A, Mouch A (2012) Vitamin D improves viral response in hepatitis C genotype 2–3 naive patients. World J Gastroenterol 18: 800–805.

32. Kondo Y, Ueno Y, Kakazu E, Kobayashi K, Shiina M, et al. (2011) Lymphotropic HCV strain can infect human primary naive CD4+ cells and affect their proliferation and IFN-gamma secretion activity. J Gastroenterol 46: 232–241.

33. Kondo Y, Machida K, Liu HM, Ueno Y, Kobayashi K, et al. (2009) Hepatitis C virus infection of T cells inhibits proliferation and enhances fas-mediated apoptosis by down-regulating the expression of CD44 splicing variant 6. J Infect Dis 199: 726–736.

34. Machida K, Kondo Y, Huang JY, Chen YC, Cheng KT, et al. (2008) Hepatitis C virus (HCV)-induced immunoglobulin hypermutation reduces the affinity and neutralizing activities of antibodies against HCV envelope protein. J Virol 82: 6711–6720.

35. Kondo Y, Sung VM, Machida K, Liu M, Lai MM (2007) Hepatitis C virus infects T cells and affects interferon-gamma signaling in T cell lines. Virology 361: 161–173.

36. Fattovich G, Covolo L, Bibert S, Askarieh G, Lagging M, et al. (2011) IL28B polymorphisms, IP-10 and viral load predict virological response to therapy in chronic hepatitis C. Aliment Pharmacol Ther 33: 1162–1172.

37. Darling JM, Aerssens J, Fanning G, McHutchison JG, Goldstein DB, et al. (2011) Quantitation of pretreatment serum interferon-gamma-inducible protein-10 improves the predictive value of an IL28B gene polymorphism for hepatitis C treatment response. Hepatology 53: 14–22.

38. Dill MT, Duong FH, Vogt JE, Bibert S, Bochud PY, et al. (2011) Interferon-induced gene expression is a stronger predictor of treatment response than IL28B genotype in patients with hepatitis C. Gastroenterology 140: 1021–1031.

39. Abe H, Hayes CN, Ochi H, Maekawa T, Tsuge M, et al. (2011) IL28 variation affects expression of interferon stimulated genes and peg-interferon and ribavirin therapy. J Hepatol 54: 1094–1101.

40. Schaalan MF, Mohamed WA, Amin HH (2012) Vitamin D deficiency: Correlation to interleukin-17, interleukin-23 and PIIINP in hepatitis C virus genotype 4. World J Gastroenterol 18: 3738–3744.

41. Sadeghi K, Wessner B, Laggner U, Ploder M, Tamandl D, et al. (2006) Vitamin D3 down-regulates monocyte TLR expression and triggers hyporesponsiveness to pathogen-associated molecular patterns. Eur J Immunol 36: 361–370.

42. Aarskog NK, Vedeler CA (2000) Real-time quantitative polymerase chain reaction. A new method that detects both the peripheral myelin protein 22 duplication in Charcot-Marie-Tooth type 1A disease and the peripheral myelin protein 22 deletion in hereditary neuropathy with liability to pressure palsies. Human genetics 107: 494–498.

The Hepatitis E Virus Capsid C-Terminal Region Is Essential for the Viral Life Cycle: Implication for Viral Genome Encapsidation and Particle Stabilization

Tomoyuki Shiota, Tian-Cheng Li, Sayaka Yoshizaki, Takanobu Kato, Takaji Wakita, Koji Ishii

Department of Virology II, National Institute of Infectious Diseases, Gakuen, Musashi-murayama, Tokyo, Japan

Although the C-terminal 52 amino acids (C52aa) of hepatitis E virus (HEV) capsid are not essential for morphology, the C52aa-encoding region is required for replication. Transfection of a C52aa knockdown mutant showed transient growth, and the earliest population included a majority of noninfectious (possibly empty) particles and a minority of infectious particles with C-terminal capsid degradation. Finally, the complete revertant was generated reproducibly. C52aa is essential for the viral life cycle, promoting accurate encapsidation and stabilizing encapsidated particles.

epatitis E virus (HEV) is responsible for acute and enterically transmitted hepatitis in the developing world (1). Before the establishment of high-efficiency HEV cell culture systems (2), *in vitro* generation of HEV virus-like particles (HEV-VLPs) in insect cells and *in vivo* propagation in nonhuman primates were the most useful models for the study of HEV. Genetic deletions or cellular processing resulting in the loss of the N-terminal 111 or 13 amino acids (aa) or of the C-terminal 52 aa (C52aa) yielded capsid protein capable of directing the formation of the HEV small (S) or large (L) VLPs (3–5). Particle formation was required for C52aa abbreviation, limiting the structural analysis of the resulting particles (3, 4, 6–10). However, the contribution of the C52aa-encoding sequence was confirmed by both *in vivo* (attenuated infectivity of the point mutant virus in nonhuman primates) and *in vitro* (reduced RNA synthesis by RNA-dependent RNA polymerase [RdRp]) assays (11–14). Furthermore, the highly conserved nature of the C52aa sequence implies that the C52aa domain itself is functionally important. In this study, we characterized the role of the C52aa domain in the HEV life cycle by using infectious clones.

We constructed infectious clones by using the infectious virus G3-HEV83-2-27, employing a procedure described previously (20). Using a synthetic cDNA as the template, we amplified 12 fragments covering the entire G3-HEV83-2-27 genome by PCR with the primers listed in Table 1. These fragments were ligated stepwise and were inserted into the EcoRI-HindIII site of pUC19, yielding a wild-type clone that we designated WT. Site-directed mutagenesis of WT was used to generate clones that were mutated to encode capsid protein lacking the C52aa domain, either by introduction of an amber stop codon, UAA (a knockdown mutant designated Amut), or via deletion of the corresponding segment of the open reading frame 2 (ORF2) sequence (a knockout mutant designated Dmut). We performed experiments on three separate scales (normal, large, and huge, as described below) in order to estimate virus progeny productivity, to clarify the growth kinetics, and to analyze the process of encapsidation in the absence of revertants.

Normal scale. To estimate the virus progeny productivity of HEV without C52aa, transfection with Amut and Dmut was performed in comparison to transfection with WT. A 50-μg quantity of RNA from each infectious clone was electroporated into 1×10^7 cells of PLC/PRF/5. Analysis by enzyme-linked immunosor-

bent assay (ELISA) (using an anti-G3-HEV-VLP rabbit polyclonal antibody [5]) suggested that transient growth was observed with Amut, in contrast to continuous growth with WT (Fig. 1A) and no growth with Dmut (data not shown). The productivity (expressed as the genome copy number) of Amut, measured by real-time reverse transcription-PCR (RT-PCR) of RNA with a set of specific primers (Table 1), was estimated as approximately 40-fold lower than that of WT (Fig. 1B and 1C; note the differences in scale). However, subsequent analysis demonstrated that the Amut-derived HEV actually harbored synonymous and nonsynonymous reversion mutations, suggesting that the actual productivity (of intact Amut) was much lower than that suggested by real-time RT-PCR. To assess the progeny, sucrose density gradient analysis (SDGA) (with a gradient from 10 to 60% [wt/vol] sucrose) was performed. Subsequently, the collected fractions were separated by sodium dodecyl sulfate-polyacrylamide gel electrophoresis (SDS-PAGE), and Western blot analysis (WB) was performed with the polyclonal antibody noted above (5). Chemiluminescence was recorded using an LAS-3000 luminescent image analyzer (Fujifilm, Tokyo, Japan). In the series of fractions obtained from progeny derived from infection with WT, the presence of antigen was confirmed only in fraction 8 (F8) in Fig. 1C by WB (data not shown). The 72-kDa size of the prominent band was in agreement with the size of the capsid protein predicted for the WT clone. Quantification of the HEV RNA genome copy number showed a trailing peak for the progeny derived from infection with Amut (Fig. 1B, F8 and F9) and a single peak for the progeny derived from infection with WT (Fig. 1C, F8). These peaks corresponded to similar specific densities. Sequence analysis showed that while the progeny from infection with WT carried the original sequence, the progeny from infection with Amut did not contain the expected UAA (amber codon) at this position. Instead, the trailing peak of this Amut-derived sample corresponded to two

— 81 —

TABLE 1 Primers used for the construction of an HEV infectious cDNA clone, the C52aa deletion mutant, and the amber mutant and for the quantification and sequencing of HEV RNA by real-time RT-PCR

Name	Polarity[a]	Sequence (5'–3')	Position in genome (nt)[b]	Amplicon (amplified region in genome [nt])[b]
ET7G2-F	+	GAATTCAATACGACTCACTATAGGCAGACCACGTATGTGGTCGAT[c]	2–23	Fragment 1-1 (2–155)
155R-EV	−	AGTCTGCACGCGAGATAAAAACGGCCGGAC	126–155	
126F-EV	+	GTCCGGCCGTTTTTATCTCGCGTGCAGACT	126–155	Fragment 1-2 (126–1370)
1370R-EV	−	CACCCTGGGATCCAGATGGAAGCCCGCAG	1342–1370	
1363F-EV	+	TCTGCGGGCTTCCATCTGGATCCCAGGGTG	1341–1370	Fragment 2-1 (1341–1794)
1816R-EV	−	ACTGCTCAGGGCCGTTCGCCTCAAGATGAG	1765–1794	
1787F-EV	+	CTCATCTTGAGGCGAACGGCCCTGAGCAGT	1765–1794	Fragment 2-2 (1765–2934)
2956R-EV	−	CGGCACAGGCACGGCCAACCTCTGTGGCAG	2905–2934	
2857F-EV	+	CCGATGCAGCCGGCACTCACAATAACGGAG	2835–2864	Fragment 3-1 (2835–3194)
3216R-EV	−	AGCCCGCTGCATATGTAATAGCAGCAAGTG	3165–3194	
3187F-EV	+	CACTTGCTGCTATTACATATGCAGCGGGCT	3165–3194	Fragment 3-2 (3165–3925)
3947R-EV	−	TCCGTAAGCTCAAAAACCAACACACTATCG	3896–3925	
3918F-EV	+	CGATAGTGTGTTGGTTTTTGAGCTTACGGA	3896–3925	Fragment 3-3 (3896–4598)
4620R-EV	−	CTTCCAAAACCCCTTAAGGGATTCCTTAGG	4569–4598	
4591F-EV	+	CCTAAGGAATCCCTTAAGGGGTTTTGGAAG	4569–4598	Fragment 4-1 (4569–5406)
5428R-EV	−	CTGTCGAGGGCGAGCTCCAGCCCCGGATTG	5377–5406	
5399F-EV	+	CAATCCGGGGCTGGAGCTCGCCCTCGACAG	5377–5406	Fragment 4-2 (5377–5851)
5873R-EV	−	TGGAGTTCATGTCAACAGAAGTAGGGGTAG	5822–5851	
5844F-EV	+	CTACCCCTACTTCTGTTGACATGAACTCCA	5822–5851	Fragment 4-3 (5822–6185)
6207R-EV	−	GTTCCATCGGCACCGCGGGCGCAGCCGATG	6157–6185	
6179F-EV	+	CATCGGCTGCGCCGCGGTGCCGATGGAAC	6157–6185	Fragment 5-1 (6157–7101)
7101R-EV	−	AGTAGACTGGAAGGCGCAACCCTGC	7077–7101	
6981F-EV	+	CTGCGGTCGGGTGTTAGCTCCACACTCGG	6959–6988	Fragment 5-2 (6959–7266)
SmartIIA-Hind	−	GCTCGAGCGGCCGCCAGTGTGATGGATATCTGCAGAATTCG GCTTAAGCAGTGGTATCAACGCAGAAAGCTTTTTTTTT TTTTTTTTTTTTTTTTTTTT[d]	7238–7266	
D81-F	+	ATGTGCCCTAGGGCTGTTCTGTTG	5173–5196	D81F/ORF2-52aa-Pac-R (5173–6995)
ORF2-52aa-Pac-R	−	AATTAATTAATTAAGCAAGGGCCGAGTGTGGAG[e]	6977–6995	
ORF2-52aa-del-F	+	TCCACACTCGGCCCTTGCTTAACTTGAGGATACTATTGACTAT[f]	6978–7020	D81-F/ORF2-52aa-del-R (5173–7020)
ORF2-52aa-del-R	−	ATAGTCAATAGTATCCTCAAGTTAAGCAAGGGCCGAGTGTGGA[f]	6978–7020	
7224R	−	AGGGAGCGCGAAAAGCAGAAAAGAAAAAT	7196–7224	ORF2-52aa-del-F/7224R (6978–7224)
HEV-G3-ANYF	+	ACCCCGGCAGTTGGTTTT	179–196	HEV-G3-ANYF/ANYR (179–234)
HEV-G3-ANYR	−	CCCGCTGGATAGGATGATTCC	212–234	
HEV-G3-ANYM1	+	FAM-CGCCCTGAGGTACTT-BHQ-1[g]	198–212	
83-2-6564F	+	GCTTCGTGCTAATGATGTTCTGTG	6564–6587	83-2-6564F/3'-terminal end (6564–7266)
83-2-6940F	+	CACCCAGGCTAGTGGTGTAGGTAGA	6940–6964	83-2-6940F/3'-terminal end (6940–7266)
ORF2-R-pacI	−	GAGAATTAAGACTCCCGGGTTTTAC	7136–7160	83-2-6564F/ORF2-R-pacI (6564–7160)

[a] Polarity of the primer on the HEV genome. +, forward; −, reverse.
[b] In G3-HEV83-2-27 (GenBank accession no. AB740232).
[c] The underlined sequence contains the T7 promoter.
[d] The underlined sequence contains a SmartIIA-specific sequence and a HindIII-digestible sequence.
[e] The underlined sequence contains a PacI-digestible sequence.
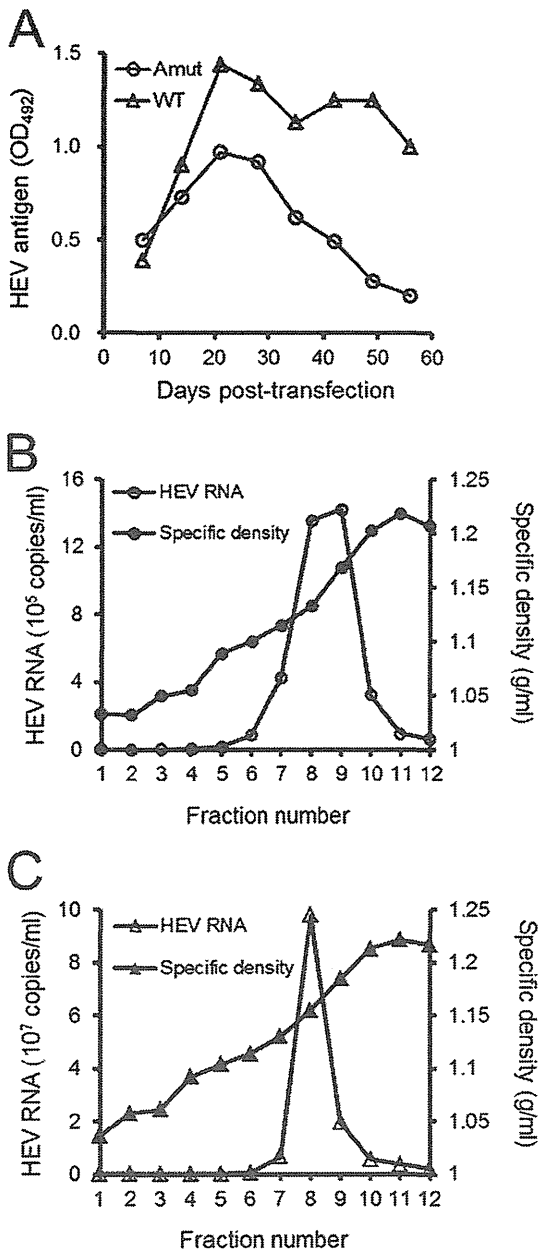[f] The mutated nucleotides are underlined.
[g] The fluorophore 6-carboxyfluorescein (FAM) is attached to the 5' end of the probe, and a quencher, Black Hole Quencher-1 (BHQ-1), is attached to the 3' end.

distinct peaks (F8 and F9) harboring the GUU (Val-encoding) and GAC (Asp-encoding) codons, respectively. These changed RNA sequences were predicted to encode full-length revertant capsid proteins.

Large scale. To clarify the precise growth kinetics of Amut, a larger-scale transfection of Amut RNA was performed. Specifically, the large-scale transfection was performed on a scale approximately 30-fold larger than that described above, and culture supernatants were collected periodically. This procedure permitted a time course of quantification by ELISA analysis and showed that the peak of antigen accumulation occurred 25 days posttransfection, while the number of viral genomes progressively declined during the 2 months of the study (except for small recoveries in copy number on day 25 and at the end of the study) (Fig. 2A). These data suggested the production of a low level of infectious particles from Amut transfection. However, the nonreverted Amut antigens could not be distinguished by WB in the normal- and large-scale experiments, suggesting that the Amut products were unstable,

of low infectivity, and/or produced in small amounts. To confirm the nature of the Amut product, pooled supernatants were subjected to partial purification and SDGA. WB of the resulting fractions detected a 72-kDa band in F7 (specific density, 1.15 g/ml) (Fig. 2B). Quantification of the HEV RNA genome in the fractions detected a single peak, primarily in F7 (Fig. 2C). Determination of the F7 sequence revealed that the codon expected to be an amber codon was instead GUC (complete reversion). Additionally, infection assays demonstrated that F7 readily infected cells (Fig. 2D). Based on our subsequent experiments, we suspect that the end product of the large-scale experiment likely corresponded to a revertant to WT.
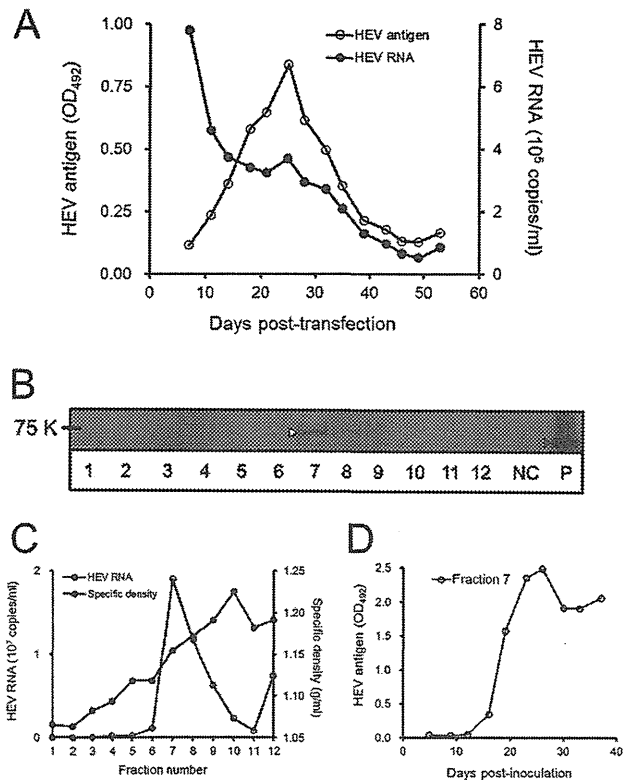
Huge scale. To clarify the apparent reversion of Amut, transfection was performed at an even larger scale (10-fold increased over the large scale); culture supernatants were collected periodically, and viral sequences from these samples were determined. The results clearly showed a population shift from the originating amber codon of Amut to the complete revertant (GUC) via an intermediate mutant (GAC) (Table 2). Reversion mutants were

– 82 –

FIG 2 Growth kinetics and character of Amut. (A) Supernatants were collected periodically during 2 months of culturing, and HEV antigen levels were measured by ELISA using an anti-G3-HEV-VLP rabbit polyclonal antibody; the HEV RNA genome copy number was determined by real-time reverse transcription-PCR. OD_{492}, optical density at 492 nm. Supernatants from a pooled total of 3 liters of culture were concentrated and sedimented. (B) Fractions were subjected to Western blotting using an anti-G3-HEV-VLP rabbit polyclonal antibody. NC, negative control (untransfected cells). P, positive control (HEV-L-VLPs). 75 K, 75,000 (molecular weight). Symbols designate the positions of the major band in the Amut supernatant (open arrowhead) and the HEV-L-VLP (filled arrowhead). (C) Fractions were assessed for the HEV RNA genome copy number and specific density. (D) Confirmation of the infectivity of fraction 7 by ELISA.

FIG 1 Initial characterization of Amut and WT HEV. (A) Time course of antigen production following transfection with Amut or WT HEV. HEV antigen levels were measured by ELISA using an anti-G3-HEV-VLP rabbit polyclonal antibody. OD_{492}, optical density at 492 nm. (B and C) Sedimentation analyses of the Amut product (B) and of the WT product, used as a control (C). Concentrated supernatants derived from 50-ml cultures were sedimented on continuous sucrose gradients (10% to 60% [wt/vol] in phosphate-buffered saline). The resulting fractions were assessed for specific density and the HEV RNA genome copy number (by real-time reverse transcription-PCR). Note the distinct y-axis scales in panels B and C.

not detected until 3 weeks posttransfection. The reproducible reversion of Amut provides evidence of the functional essentiality of the C52aa domain for the HEV life cycle.

To permit analysis of the Amut clone in the absence of revertants, culture supernatants collected within the first 10 days were pooled and subjected to partial purification and SDGA. WB detected multiple bands of approximately 55 kDa and smaller, starting in F7; these bands formed a broad range, with peak accumulation detected in F10 (specific density, 1.21 g/ml) (Fig. 3A). In contrast, F8 (specific density, 1.15 g/ml) had the highest copy number of the genome (Fig. 3B). For subsequent analysis, F8 and F10 were designated the minor and major products (Mip and Map, respectively) based on antigen levels. To determine the RNase sensitivities of the products, the fractions were treated with 20 μg/ml of RNase A for 30 min at 37°C. The RNase resistance of the fractions was confirmed by RT-PCR quantification analysis, indicating viral encapsidation. Both products exhibited resistance to RNase treatment (Fig. 3C), indicating the presence of encapsidated RNA. Neither the GAC nor the GUC reversion mutation was detected in these products by RT-PCR sequencing analysis, suggesting that those specific alleles were largely absent from this population.

Further analysis of peak discrepancy between the antigen level and the genome copy number revealed two points. First, the copy

– 83 –

TABLE 2 Time course sequence of the codon mutated to an amber codon for the supernatants of Amut-transfected cells

Codon	Sequence[a] at the following day posttransfection:								
	7	10	14	17	21	24	28	31	35
Amber mutant	UAA	UAA	UAA	UAA	UAA	ND	ND	ND	ND
Revertant									
Intermediate	ND	ND	ND	ND	ND	GAC	GAC	ND	ND
Complete	ND	ND	ND	ND	ND	GUC	GUC	GUC	GUC

[a] Determined for the first codon of the C52aa-encoding region of the ORF2 gene. ND, not detected.

number in the Map fraction was approximately 15 times lower than that in the Mip fraction (Fig. 3B). Second, the constitution (genome/antigen) ratio in the Map fraction was approximately 40-fold lower than that in the Mip fraction by analysis using Image Gauge, version 4.0 (Fujifilm, Tokyo, Japan); the ratio in the Mip fraction was approximately equal to that of WT (Fig. 3D). On the other hand, the RNA content of the Map fraction was extremely reduced, suggesting that these products represented empty parti-
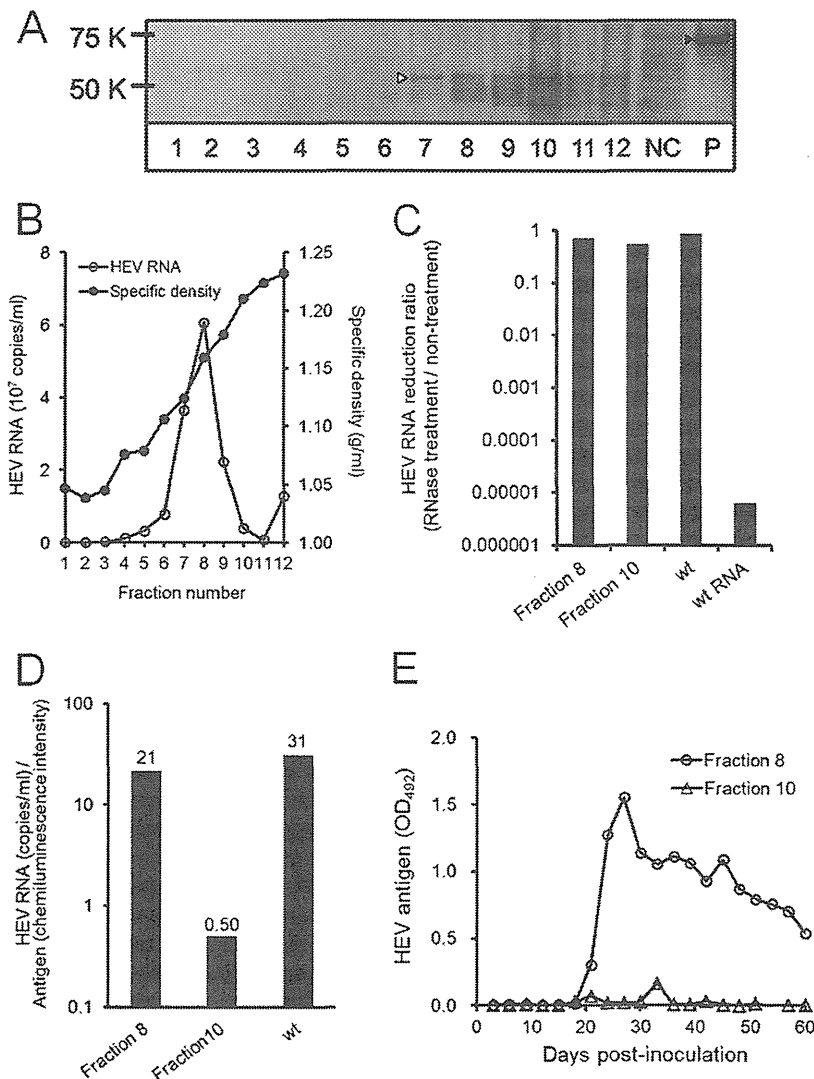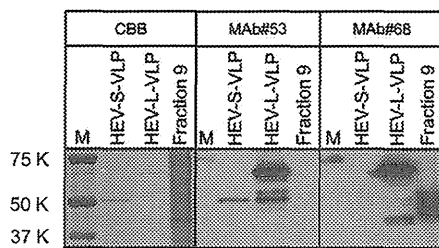

FIG 3 Encapsidation of the Amut genome and its characteristics. (A) Fractions were subjected to Western blotting using an anti-G3-HEV-VLP rabbit polyclonal antibody. NC, negative control (uninfected cells). Symbols indicate the positions of the major bands in the Amut fraction (55 kDa) (open arrowhead) and the WT fraction, used as a positive (P) control (72 kDa) (filled arrowhead). (B) Fractions were assessed for the HEV RNA genome copy number and specific density. (C) RNase resistance was measured as the ratio of the level of HEV RNA in RNase-treated fractions to that in untreated fractions (HEV RNA reduction ratio). WT virions and extracted WT RNA were used as positive and negative controls, respectively. (D) Constitution (genome/antigen) ratios (actual values are shown above the bars) were calculated by dividing the genome quantities from panel B by the chemiluminescence intensities from panel A. (E) To confirm the infectivity of the indicated fractions, cells were inoculated and periodically analyzed by ELISA using an anti-G3-HEV-VLP rabbit polyclonal antibody. OD_{492}, optical density at 492 nm.

– 84 –

CBB			MAb#53			MAb#68		
M	HEV-S-VLP	HEV-L-VLP	Fraction 9	M	HEV-S-VLP	HEV-L-VLP	Fraction 9	M	HEV-S-VLP	HEV-L-VLP	Fraction 9

75 K
50 K
37 K

FIG 4 Detection of degraded capsid termini in Amut. HEV small virus-like particles (HEV-S-VLP), HEV large virus-like particles (HEV-L-VLP), and fraction 9 (derived as described for Fig. 3A) were stained with Coomassie brilliant blue (CBB) or were subjected to Western blot analysis using a monoclonal antibody specific to both HEV-S-VLP and HEV-L-VLP (MAb 53) or to HEV-L-VLP alone (MAb 68). Lane M, molecular weight markers.

cles; this inference is consistent with the low productivity of Amut products on all scales. Specifically, we observed that the Map fraction could not infect cells (Fig. 3E), while the Mip fraction was infectious for these cells (Fig. 3E) and yielded reversion mutants (GUC) during long-term observation (data not shown). While the viral reproduction of Amut was impaired, the Mip fraction could sustain low levels of viral production, leading to the emergence of revertants as shown in the large-scale experiment (Fig. 2A).

The observation, via WB (Fig. 3A), of a "smear" of antigen with a maximum size of 55 kDa was unexpected, given that the capsid protein lacking C52aa (predicted size, 6 kDa) was expected to migrate at 66 kDa (that is, 72 kDa less 6 kDa). The observed 11-kDa decrease in size suggested further degradation of the capsid in the absence of the C52aa domain. Mass spectroscopy followed by protein sequencing detected two fragments with amino acid sequences corresponding to early N-terminal capsid sequences. The presence of the capsid N-terminal domain was confirmed by detection with monoclonal antibody (MAb) 68 (Fig. 4), a reagent that exhibits specificity for HEV-L-VLP (specific to the N-terminal 13 to 111 aa) (T. C. Li, unpublished observations). In contrast, the protein was not detected using the HEV-S-VLP- and HEV-L-VLP-specific MAb 53 (Fig. 4), implying the absence of the S-and-L common region. Protein sequencing and reactivity with the HEV-VLP-specific antibodies strongly suggested that the 55-kDa bands correspond to proteolytic products generated by degradation from the C terminus on the viral surface, presumably via loss of the P domain. Further degradation (to lower-molecular-weight species) probably occurred after encapsidation, given that previous studies showed that this region was essential for dimerization and particle formation by the capsid (3, 15, 16).

HEV virions exhibit distinct buoyant densities in feces (1.26 to 1.27 g/ml) and in circulating blood (1.15 to 1.16 g/ml), differences that might be associated with their cellular membrane content (17). The density of the Amut Map fraction was higher than that of the Mip fraction. This result is inconsistent with the notion that the Map is an empty particle (18). The Amut Mip fraction had the specific density of membrane-associated virions, although the ORF3 (egress-related) protein was not detected in these particles, in contrast to WT particles (T. Shiota, unpublished observations) (19). We hypothesize that the correct encapsidation of Amut resulted in an enveloped particle lacking the ORF3 protein (Mip; density, 1.15 g/ml), whereas the incorrect encapsidation of Amut resulted in an nonenveloped and

(usually) empty particle (Map; density, 1.21 g/ml), the density of which was intermediate between that of the membrane-associated virion (1.15 to 1.16 g/ml) and the nonenveloped filled virion (1.26 to 1.27 g/ml) (17).

In the present study, we showed that the C52aa domain of the HEV capsid was essential for the HEV life cycle, as confirmed by reproducible reversion at the amber mutation, which would otherwise truncate the C52aa domain. The presence of the C52aa domain promoted the accurate encapsidation of HEV and protected the particle from further C-terminal degradation. To clarify the involvement of the C52aa domain in neutralization, further studies (e.g., using a MAb specific for this region) will be required.

ACKNOWLEDGMENTS

REFERENCES

1. Chandra V, Taneja S, Kalia M, Jameel S. 2008. Molecular biology and pathogenesis of hepatitis E virus. J. Biosci. 33:451–464.
2. Tanaka T, Takahashi M, Kusano E, Okamoto H. 2007. Development and evaluation of an efficient cell-culture system for hepatitis E virus. J. Gen. Virol. 88:903–911.
3. Li TC, Takeda N, Miyamura T, Matsuura Y, Wang JC, Engvall H, Hammar L, Xing L, Cheng RH. 2005. Essential elements of the capsid protein for self-assembly into empty virus-like particles of hepatitis E virus. J. Virol. 79:12999–13006.
4. Xing L, Li TC, Mayazaki N, Simon MN, Wall JS, Moore M, Wang CY, Takeda N, Wakita T, Miyamura T, Cheng RH. 2010. Structure of hepatitis E virion-sized particle reveals an RNA-dependent viral assembly pathway. J. Biol. Chem. 285:33175–33183.
5. Li TC, Yamakawa Y, Suzuki K, Tatsumi M, Razak MA, Uchida T, Takeda N, Miyamura T. 1997. Expression and self-assembly of empty virus-like particles of hepatitis E virus. J. Virol. 71:7207–7213.
6. Mori Y, Matsuura Y. 2011. Structure of hepatitis E viral particle. Virus Res. 161:59–64.
7. Xing L, Kato K, Li T, Takeda N, Miyamura T, Hammar L, Cheng RH. 1999. Recombinant hepatitis E capsid protein self-assembles into a dual-domain T=1 particle presenting native virus epitopes. Virology 265:35–45.
8. Guu TS, Liu Z, Ye Q, Mata DA, Li K, Yin C, Zhang J, Tao YJ. 2009. Structure of the hepatitis E virus-like particle suggests mechanisms for virus assembly and receptor binding. Proc. Natl. Acad. Sci. U. S. A. 106:12992–12997.
9. Yamashita T, Mori Y, Miyazaki N, Cheng RH, Yoshimura M, Unno H, Shima R, Moriishi K, Tsukihara T, Li TC, Takeda N, Miyamura T, Matsuura Y. 2009. Biological and immunological characteristics of hepatitis E virus-like particles based on the crystal structure. Proc. Natl. Acad. Sci. U. S. A. 106:12986–12991.
10. Xing L, Wang JC, Li TC, Yasutomi Y, Lara J, Khudyakov Y, Schofield D, Emerson SU, Purcell RH, Takeda N, Miyamura T, Cheng RH. 2011. Spatial configuration of hepatitis E virus antigenic domain. J. Virol. 85:1117–1124.
11. Agrawal S, Gupta D, Panda SK. 2001. The 3' end of hepatitis E virus (HEV) genome binds specifically to the viral RNA-dependent RNA polymerase (RdRp). Virology 282:87–101.
12. Emerson SU, Zhang M, Meng XJ, Nguyen H, St Claire M, Govindarajan S, Huang YK, Purcell RH. 2001. Recombinant hepatitis E virus genomes infectious for primates: importance of capping and discovery of a cis-reactive element. Proc. Natl. Acad. Sci. U. S. A. 98:15270–15275.
13. Graff J, Nguyen H, Kasorndorkbua C, Halbur PG, St Claire M, Purcell RH, Emerson SU. 2005. In vitro and in vivo mutational analysis of the 3'-terminal regions of hepatitis E virus genomes and replicons. J. Virol. 79:1017–1026.
14. Kumar A, Panda SK, Durgapal H, Acharya SK, Rehman S, Kar UK. 2010. Inhibition of hepatitis E virus replication using short hairpin RNA (shRNA). Antiviral Res. 85:541–550.

– 85 –

15. Li SW, Zhang J, He ZQ, Gu Y, Liu RS, Lin J, Chen YX, Ng MH, Xia NS. 2005. Mutational analysis of essential interactions involved in the assembly of hepatitis E virus capsid. J. Biol. Chem. 280:3400–3406.

16. Graff J, Zhou YH, Torian U, Nguyen H, St Claire M, Yu C, Purcell RH, Emerson SU. 2008. Mutations within potential glycosylation sites in the capsid protein of hepatitis E virus prevent the formation of infectious virus particles. J. Virol. 82:1185–1194.

17. Takahashi M, Tanaka T, Takahashi H, Hoshino Y, Nagashima S, Jirintai, Mizuo H, Yazaki Y, Takagi T, Azuma M, Kusano E, Isoda N, Sugano K, Okamoto H. 2010. Hepatitis E virus (HEV) strains in serum samples can replicate efficiently in cultured cells despite the coexistence of HEV antibodies: characterization of HEV virions in blood circulation. J. Clin. Microbiol. 48:1112–1125.

18. Jacobson MF, Baltimore D. 1968. Morphogenesis of poliovirus. I. Association of the viral RNA with coat protein. J. Mol. Biol. 33:369–378.

19. Tyagi S, Korkaya H, Zafrullah M, Jameel S, Lal SK. 2002. The phosphorylated form of the ORF3 protein of hepatitis E virus interacts with its non-glycosylated form of the major capsid protein, ORF2. J. Biol. Chem. 277:22759–22767.

20. Li T-C, Song S, Yang Q, Ishii K, Takeda N, Wakita T. 2011. A cell culture system for hepatitis E virus. Hepatol. Int. 5:202. doi:10.1007/s12072-010-9241-z.

— 86 —
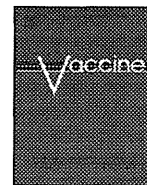
Influenza A whole virion vaccine induces a rapid reduction of peripheral blood leukocytes via interferon-α-dependent apoptosis

Manabu Ato [a,*], Yoshimasa Takahashi [a], Hideki Fujii [a,1], Shu-ichi Hashimoto [a,2], Tomohiro Kaji [a,b], Shigeyuki Itamura [c], Yoshinobu Horiuchi [d,e], Yoshichika Arakawa [d,3], Masato Tashiro [c], Toshitada Takemori [a,b]

[a] Department of Immunology, National Institute of Infectious Diseases, Toyama 1-23-1, Shinjuku-ku, Tokyo 162-8640, Japan
[b] Laboratory for Immunological Memory, Riken Research Center for Allergy and Immunology, Suehiro-cho 1-7-22, Tsurumi-ku, Yokohama, Kanagawa 230-0045, Japan
[c] Influenza Virus Research Center, National Institute of Infectious Diseases, Gakuen 4-7-1, Musashi-Murayama, Tokyo 208-0011, Japan
[d] Department of Bacteriology II, National Institute of Infectious Diseases, Gakuen 4-7-1, Musashi-Murayama, Tokyo 208-0011, Japan
[e] Division of Quality Assurance, National Institute of Infectious Diseases, Gakuen 4-7-1, Musashi-Murayama, Tokyo 208-0011, Japan

ARTICLE INFO

ABSTRACT

Infection with single strand RNA (ssRNA) viruses, such as influenza A virus, is known to induce protective acquired immune responses, including the production of neutralizing antibodies. Vaccination also causes a reduction in the number of peripheral blood leukocytes (PBL) shortly after inoculation, a result which may have undesirable adverse effects. The cellular mechanisms for this response have not been elucidated so far. Here we report that formalin-inactivated influenza A whole virus vaccine (whole virion) induces a significant decrease in PBL in mice 5–16 h after administration, whereas an ether-split vaccine (HA split) made from the same influenza virus strain does not induce a similar loss of PBL. Concordant with this reduction in the number of PBL, a rapidly induced and massive production of interferon (IFN)-α is observed when mice are injected with whole virion, but not with HA split vaccines. The role of Toll-like receptors (TLR), which are involved in signal transduction of influenza virus, and the subsequent induction of IFNα were confirmed using mice lacking TLR7, MyD-88, or IFNα/β receptor. We further demonstrated that the observed PBL loss is caused by apoptosis in an IFNα-dependent manner, and not by leukocyte redistribution due to chemokine signaling failure. These findings indicate that RNA-encapsulated whole virion vaccines can rapidly induce a loss of leukocytes from peripheral blood by apoptosis, which may modulate the subsequent immune response.

© 2013 Elsevier Ltd. All rights reserved.

1. Introduction

Viral infection or vaccination is known to elicit a rapid and robust innate immune response by the host. Activation of the innate immune system is believed to play a key role in host protection against infection by inducing cytokines and chemokines, recruiting leukocytes at the site of infection, and the subsequent activation of adaptive immune responses [1]. On the contrary, some viral infections and vaccinations have immunosuppressive effects, such as the loss of peripheral blood leukocytes (PBL), decreased lymphocyte numbers in the secondary lymphoid organs and immune cell apoptosis, which may result in the suppression of protective immune responses or unsuccessful vaccination [2–5].

Influenza A virus infection [6] or administration of inactivated influenza vaccine [7] can induce an acute and transient lymphocytopenia, suggesting that the activation of innate immune responses may be associated with the loss of PBL. Recent studies have demonstrated that innate immunity activation is dependent on the recognition of pathogen-specific molecular patterns (PAMPs)

[1,8]. Influenza virus-specific PAMPs are known to be detected by Toll-like receptors (TLR) 3, 7, and 8 [9,10], members of the retinoid acid-inducible gene-I (RIG-I)-like receptors, and Nod-like receptors that recognize viral RNA in the cytoplasm during viral replication [9,11,12]. Stimulation of these receptors triggers induction of type-I interferons (IFNs).

Type-I IFNs, which make up a large family including IFNβ and more than 10 members of IFNα in mammals, share a single receptor IFNα/βR, and play a major role in protecting host cells from viral infections [13]. Type-I IFNs function not only to directly inhibit viral replication, but also to modulate the subsequent immune response by inducing a large number of IFN-inducible molecules, including chemokines [14]. These in turn activate macrophages, dendritic cells, and NK cells, as well as mediate the generation of CTL [15] and antibody-producing cells [16]. Hence, inoculation of live virus or vaccine can modify the activation state and distribution of leukocytes, which may in turn modulate the intensity of virus-specific adaptive immune responses. However, it has not been clarified which particular effect is dependent on the type of vaccine and what viral component induces each host response.

Here we attempted to unravel the mechanisms of these host effects, as induced by either inactivated influenza whole virion vaccine (whole virion) or ether-split vaccine (HA split). Whole virion induces PBL loss concomitant with IFNα production. Mice deficient in IFNα/βR or MyD-88 completely retain PBL after inoculation with whole virion. We further demonstrate that this PBL loss is independent of PBL redistribution, but is instead caused by IFNα-dependent apoptosis of circulating PBL.

2. Materials and methods

2.1. Mice

C57BL/6 (B6) and outbred ddY mice were purchased from Japan SLC and were housed at the National Institute of Infectious Diseases under specific pathogen-free conditions. IFNαβR deficient mice were purchased from B&K Ltd., and backcrossed to the B6 background (B6.IFNα/βR KO) under barrier conditions. MyD-88 deficient mice and TLR7 deficient mice were kindly provided by Dr. Shizuo Akira (Osaka University). All animal procedures were performed in accordance with the guidelines of the Institutional Animal Care and Use Committee, National Institute of Infectious Diseases.

2.2. Influenza virus vaccines

Inactivated influenza whole virion and HA split vaccines were prepared from the vaccine strain A/Wyoming/3/2003 (IVR-134) (H3N2) by the Chemo-Sero-Therapeutic Research Institute, a licensed manufacturer of influenza vaccine in Japan. Briefly, the virus was propagated in the allantoic cavity of embryonated hen's eggs, and pelleted using ultracentrifugation. The pelleted virus was resuspended, further purified by zonal centrifugation with a sucrose density gradient, and inactivated with formalin for the preparation of the whole virion vaccine [17]. To prepare the HA split vaccine, the purified virus was treated with ether and polysorbate 80, and the resulting aqueous solution was recovered [18]. Inactivation was confirmed by the absence of detectable hemagglutination activity following inoculation of the vaccines into embryonated hen's eggs. Each vaccine preparation was formulated to contain a final concentration of immunologically active HA of 90 μg/ml by the use of single-radial-immunodiffusion (SRD) assays.

2.3. Administration of inactivated virus vaccine

Mice were injected i.p. at 6 weeks of age with 500 μl of whole virion or HA split in saline at a concentration of 90 μg/ml HA. For in vivo treatment with pertussis toxin (PTX), mice were injected i.p. with 500 ng of PTX (Sigma–Aldrich) or the same amount of non-functional B-oligomer of PTX (Sigma–Aldrich) as a control on the day before vaccination as previously described [19].

2.4. Flow cytometry

Ten μl of blood from the tail vein was harvested in PBS containing 0.05% heparin (Mochida Pharmaceutical). After erythrolysis by treatment with hypotonic sodium ammonium chloride buffer, the FcγR on PBL were blocked with anti-FcγRII/III mAb (2.4G2), and the cells were stained with fluorescein isothiocyanate (FITC)-labeled anti-B220 (RA3-6B2), phycoerythrin (PE)-labeled anti-CD3ε (2C11), allophycocyanin (APC) or Pacific blue-labeled anti-Ly-6C/G (RB6-8C5) mAb, (eBioSciences), and propidium iodide (PI; Sigma–Aldrich). The absolute PBL number was determined and PBL subsets were analyzed using a FACSCalibur (BD Biosciences). In some experiments, PBL were further stained with APC-labeled annexin-V (BD PharMingen) for detecting apoptotic cells.

2.5. Enzyme-linked immunosorbent assay (ELISA).

Sera from vaccinated mice were collected from the tail vein or by cardiac puncture under anesthesia. The level of cytokines in sera was measured using a Ready-Set-Go! ELISA assay kit (for TNF, IL-1α, IL-12p70; eBioscience) or mouse type-I IFNs ELISA kit (for IFNα and IFNβ; PBL) according to the manufacturers' instructions.

2.6. Anti-influenza virus antibodies

One hundred μl of sera were collected from the tail veins of individual mice at the time points indicated in the text. Anti-influenza virus Ab titers were estimated by ELISA assays using whole virion or HA split vaccine as the coating antigen [20].

3. Results

3.1. Inactivated influenza A virus but not HA split vaccine causes a loss of PBL

First, we investigated the ability of whole virion and HA split, both derived from the same vaccine strain of influenza virus A/Wyoming/3/2003 (IVR-134) (H3N2), to decrease the number of PBL. The HA protein content in each vaccine was standardized using an SRD assay, a potency assay currently used for inactivated influenza vaccine. Fig. 1A shows that the total number of PBL in a 10 μl aliquot of blood was decreased in mice shortly after immunization with the whole virion in a dose-dependent manner, but this effect was not seen with the HA split or saline inoculations ($P < 0.05$). Strikingly, whole virion vaccination induced a dose dependent decrease in the number of T- and B-cells (Fig. 1B and C), and to a lesser extent, granulocytes (Fig. 1D). However, administration of HA split vaccine did not induce a significant decrease of total PBL or any of the subpopulations. The decrease in PBL numbers after inoculation of whole virus particles was seen not only in outbred ddY mice but also in inbred strains such as B6 and BALB/c (data not shown). These findings suggest that the administration of whole virus particles causes a rapid decrease of PBL, as also seen in live influenza virus infection [4,6] and following administration of a viral RNA analog, polyinocinic-polycytidylic acid (poly (I:C)) [21], whereas administration of HA split vaccines do not affect PBL numbers.
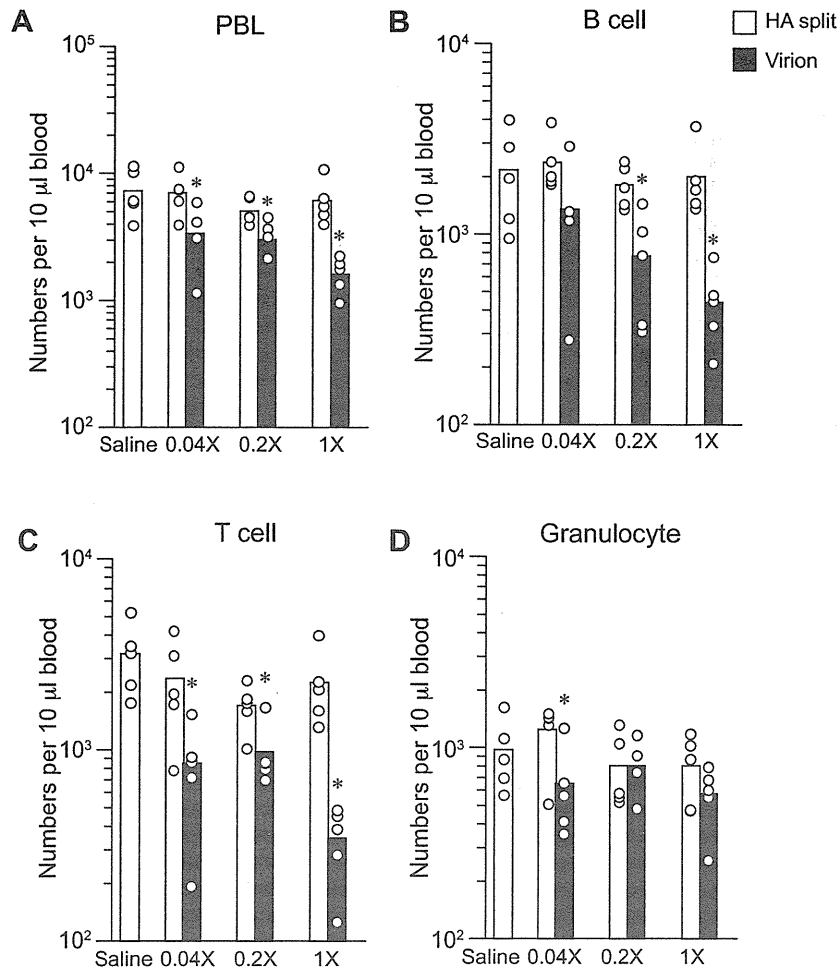
Fig. 1. Effect of inactivated influenza A vaccines on the number of PBL and of leukocyte subsets. ddY mice were injected i.p. with saline, HA split (open column) or inactivated whole virion (closed column) vaccines. The starting dose was 0.5 ml, which had been adjusted to contain the same quantity of immunologically active HA in both vaccines, with a series of dilutions as indicated. Ten μl of blood from the tail vein was collected at 16 h after inoculation. Cells were stained with PI, anti-Gr-1, anti-B220, and anti-CD3 Abs, and analyzed using flow cytometry to identify leukocyte subsets. A summary of the number of peripheral blood leukocytes (PBL) (A), B cells (B), T cells (C), and granulocytes (D) of vaccine- and saline-administrated mice is shown. Dots indicate individual values and columns indicate mean values ($n = 5$). *$P < 0.05$.

3.2. Ab response to influenza virus is independent of the decrease of PBL

Next, we examined the influence of PBL loss on acquired immune responses against influenza A virus. We measured the titer of influenza virus-specific antibody in the sera of whole virion-immunized or HA split-immunized mice. As shown in Fig. 2, we evaluated primary Ab responses by ELISA at 10 days, 30 days, and 50 days post immunization with three vaccine doses. There was no significant difference in virus-specific IgG1 titers between whole viral- and HA split- immunized mice (Fig. 2). These data indicate that the HA content measured by SRD assay for determining the vaccine doses correlated well with the in vivo virus-specific Ab responses.
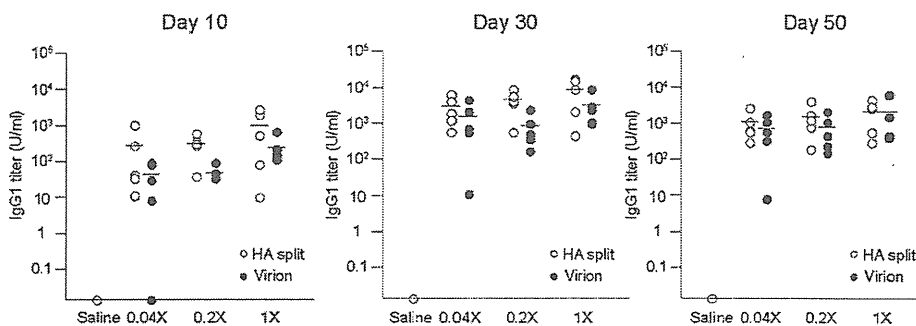
Fig. 2. Anti-influenza virus immune responses induced by immunization with whole virion and HA split vaccines. ddY mice were injected i.p. with HA split (○) and whole virion (●) vaccines with the same condition as in Fig. 1. Sera from peripheral blood were collected on the indicated days post immunization. The titers of IgG1 Abs were measured by influenza virus-specific ELISA. Bars indicate mean values ($n = 5$).

— 89 —
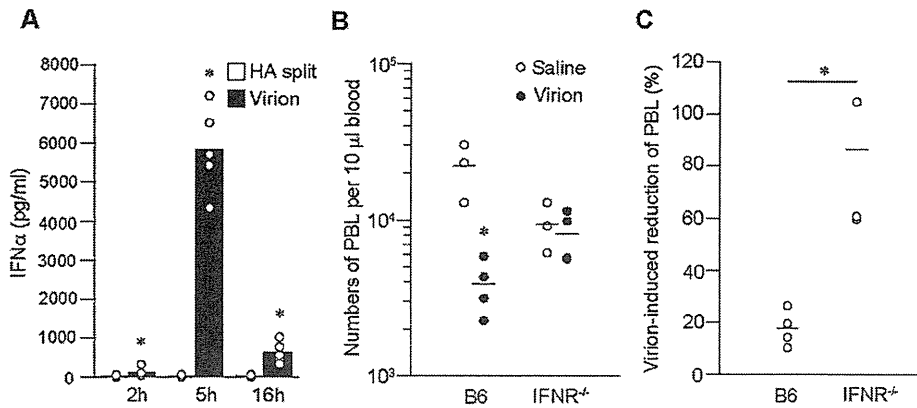
Fig. 3. The increased level of IFNα is responsible for the decreased number of PBL after administration of whole virion vaccine. (A) Sera were collected at the time points indicated from tail veins of mice that were injected i.p. with HA split (○) or whole virion (●) vaccines. The concentration of IFNα was determined by ELISA. Bars indicate mean values ($n = 5$) *$P < 0.05$. (B) Wild type C57BL/6 mice and B6.IFNα/βR KO mice were injected i.p. with 0.5 ml of saline or inactivated influenza virus; 16 h later, 10 μl of blood was collected from the tail vein. Absolute numbers of PBL (B) and the proportions of PBL in virion-administrated mice to those in mock treated mice (C) are shown. Bars indicate mean values ($n = 5$). *$P < 0.05$.

### 3.3. Loss of PBL was correlated with a high level of serum IFNα

Next, we explored which molecule is associated with PBL loss during innate immune response activation. We measured the serum levels of TNF, IL-1α, and IL-12, at 2, 5, and 16 h post inoculation, but we could not detect significant levels of those molecules with either vaccination protocol (data not shown). On the other hand, serum IFNα was detectable at 2 h post inoculation, peaked at 5 h, and was sustained even at 16 h in whole virion administrated mice (Fig. 3A). On the contrary, mice given the HA split vaccine did not produce significant IFNα. The kinetics of IFNβ concentration in sera were similar to those of IFNα (Supplementary Fig. 1). These findings indicate that the increased level of serum IFNα and IFNβ are associated with innate immune responses after administration of whole virions.

In order to evaluate whether the PBL decrease is mediated by IFNα signaling, whole virion vaccine was administrated to mice lacking the IFNα/β receptor gene (B6.IFNα/βR KO mice). Unmanipulated B6.IFNα/βR KO mice had a similar PBL profile as wild type (WT) B6 mice, including T-cell, B-cell, conventional dendritic cells, and plasmacytoid dendritic cells (pDC) in their blood and spleens (data not shown). Fig. 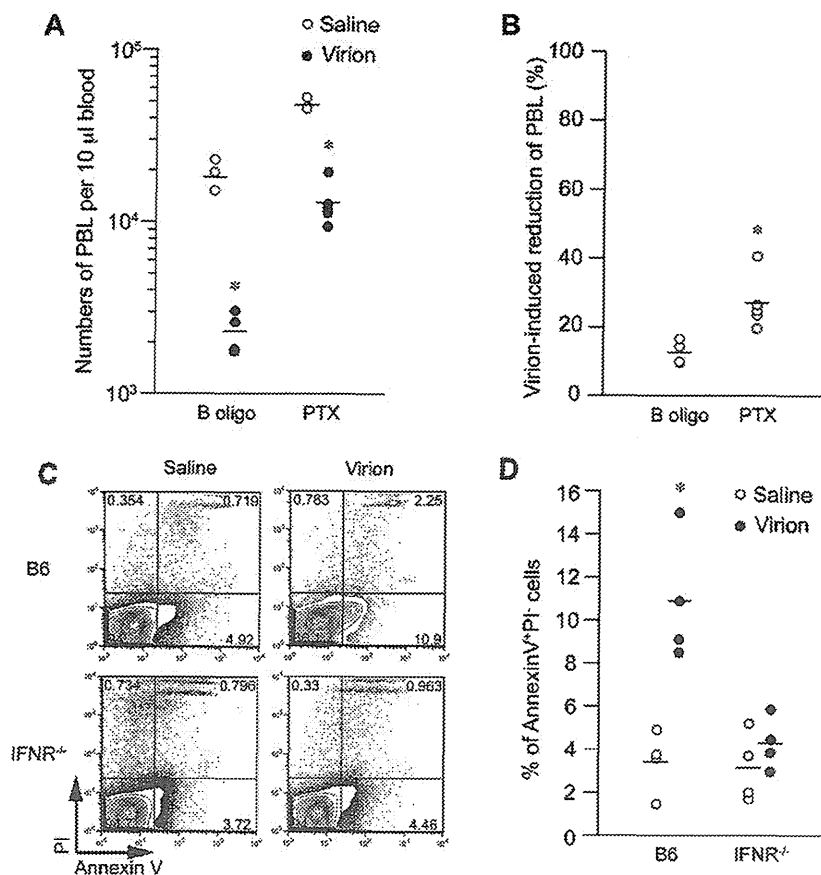3B and C show that administration of whole virion resulted in a significant reduction in the number of PBL in WT B6 mice but not in IFNα/βR KO mice. These results suggest that the loss of PBL following administration of whole virion is associated with IFNα signaling through the IFNα/βR.

3.4. TLR signaling is necessary for the loss of PBL after inoculation of influenza vaccine

As data on Fig. 3 raise the possibility that innate immune responses are responsible for the decrease of PBL numbers, we tried to define which recognition units mediate the loss of PBL occurring with inactivated influenza virus. To this end, whole virions were administrated to B6 background mice deficient in MyD-88 or TLR7, molecules that are potentially involved in signal transduction of influenza virus-mediated IFNα expression. In contrast to WT mice, which had about an 80% reduction in PBL numbers at 16 h after injection of whole virions, B6.MyD-88 KO mice showed no decrease (Fig. 4B). On the other hand, B6.TLR7 KO mice exhibited a significant but less severe (~60%) PBL reduction (Fig. 4A, C). These results suggest that whole virions cause PBL loss via a MyD-88-dependent pathway, whereas TLR7 partially contributes.
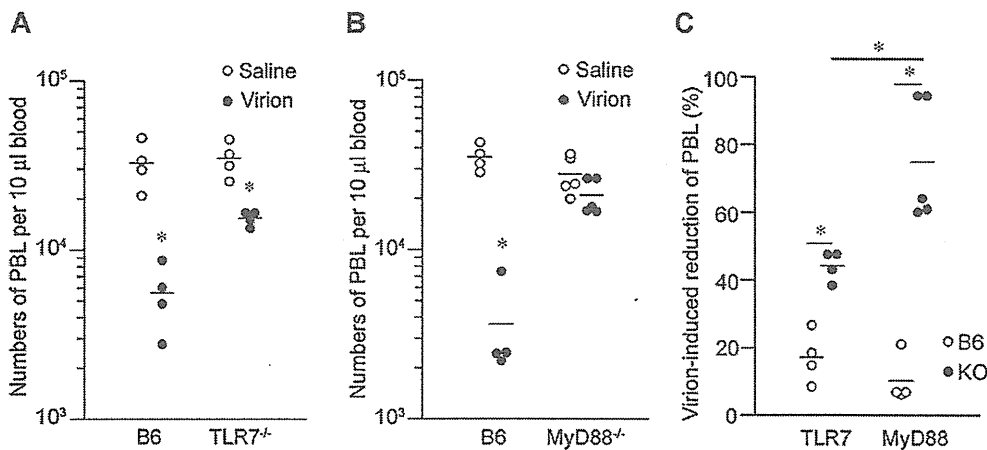
Fig. 4. TLR signaling contributes to the loss of PBL after inoculation with influenza vaccines. C57BL/6 mice, B6.TLR7 KO mice (A), or B6.MyD-88 KO mice (B) were injected i.p. with 0.5 ml of whole virion vaccine. After 16 h, 10 μl of blood was collected from the tail vein and cells were analyzed by flow cytometry. Absolute number of PBL (A, B) and the proportion of PBL in virion-administrated mice to those in mock treated mice (C) are shown. Bars indicate mean values ($n = 4$ or 5). *$P < 0.05$.

Fig. 5. Loss of PBL by apoptosis but not by redistribution after administration of whole virion. (A, B) C57BL/6 mice were injected i.p. with 0.5 ml of saline (○) or whole virion vaccine (●) along with 500 ng of pertussis toxin or control B oligomer. After 16 h, 10 μl of blood was collected from the tail vein and cells were analyzed by flow cytometry. Absolute PBL number (A) and the proportion of PBL in virion-administrated mice to those in control mice (B) are shown. Bars indicate mean values ($n = 5$). *$P < 0.05$. (C, D) Mice were injected i.p. with 0.5 ml of saline or whole virion vaccine. After 5 h, peripheral blood was collected. Cells were stained with APC-Annexin-V and PI and analyzed by flow cytometry. (C) The numbers in the plots represent the proportion of early apoptotic cells (lower right quadrant) and late apoptotic/necrotic cells (upper right quadrant) to total PBL. (D) The proportion of Annexin V⁺ PI⁻ early apoptotic cells in the PBL of saline- (○) or whole virion vaccine- (●) treated wild type C57BL/6 mice and B6.IFNα/βR KO mice. Bars indicate mean values ($n = 5$). *$P < 0.05$.

### 3.5. Apoptosis is the major mechanism of PBL loss caused by inactivated influenza virus

Next, we approached the underlying mechanisms by which PBL numbers decrease in response to inactivated influenza virus. A previous study has suggested that lymphocytes are trapped in the regional lymph nodes by Sphingosin-1-phosphate (S1P) signaling in the case of live viral infection or poly (I:C) administration [22]. To test this possibility, we administrated PTX, an inhibitor of G protein (Gαi)-coupled receptors for chemokines, including S1P, prior to vaccination of wild type or IFNα/βR KO mice with whole virions. PTX treatment failed to block the PBL decrease in WT mice at 16 h after inoculation of viral particles (Fig. 5A), although the extent of PBL reduction in PTX-treated mice was slightly less than that in the controls (Fig. 5B). These results indicate that GTP-coupled receptors regulating PBL movement do not play a definitive role in the loss of PBL. Therefore, we examined the role of cell death and examined the frequency of apoptosis and necrosis in PBL after administration of whole virions. At 5 h after inoculation, a significant loss of PBL was observed in wild type but not IFNα/βR KO mice (data not shown), which is similar to that seen at 16 h after virus administration (Fig. 3B). Of note, the proportion of Annexin-V⁺ positive apoptotic cells was elevated in the PBL from WT mice with virus administration, whereas no significant increase in the

apoptotic cell fraction was observed in PBL from B6.IFNα/βR KO mice, or from mock treated mice (Fig. 5C, D). PBL apoptosis was seen at 16 h after inactivated virus inoculation in wild type mice, though the frequency was reduced (Supplementary Fig. 2). Taken together, these data indicate that the loss of PBL after inactivated influenza virus immunization is attributable to apoptosis via IFNα/βR signaling and not to chemoattractant-dependent redistribution.

3.6. Ab response to influenza virus is dependent on IFNα signaling

To evaluate the possible role of IFNα in the establishment of humoral immunity against the influenza vaccine, we further analyzed the ability of IFNα/βR deficient mice to generate virus-specific IgG responses. IgG1 and IgG2c Ab titers were significantly impaired at the early phase after vaccination of B6.IFNα/βR KO mice as compared to wild type mice (Fig. 6, $P < 0.05$). However, at 29 days post vaccination the Ab responses were equivalent in the two mouse strains. These results indicate that IFNα/βR signaling may be necessary for rapid induction of the initial protective IgG response but not to maintain IgG titers against influenza virus.

A   **B**
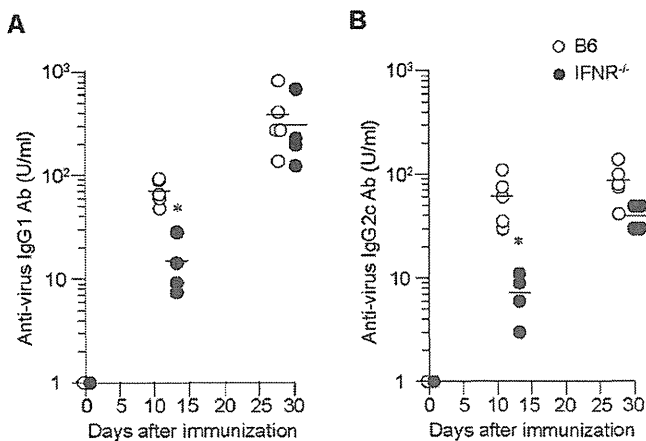
Fig. 6. The role of IFNα signaling in anti-influenza virus IgG responses to whole virion vaccine. Inactivated whole virion was administrated i.p. to wild type C57BL/6 mice (○) and B6.IFNα/βR KO mice (●) using the same conditions as Fig. 2. Sera were collected at days after immunization as indicated. The serum levels of (A) virus-specific IgG1 and (B) IgG2c antibodies were evaluated by ELISA. Bars indicate mean values ($n = 5$). *$P < 0.05$.

4. Discussion

It has been reported that the inactivated whole virion vaccine was much more effective at inducing protective immunity to influenza virus than the ether-split HA vaccine, because the former contains viral ssRNA that can activate innate immunity via TLR-7/8 signaling [23,24]. However, the precise mechanism of vaccine-induced unwanted adverse reactions, which are mainly due to excessive immune responses, is not fully understood. In this study, we immunized mice with two types of available influenza vaccines, whole virion and HA split, adjusted to contain the same quantity of immunologically active HA in both groups. To our knowledge, this is the first study demonstrating that the administration of whole virion, but not the HA split vaccine, has the potential to reduce the number of PBL in a type-I IFN signaling-dependent manner. This phenomenon is not only recognized in mice but could be reproduced in humans, because previous studies have shown that the administration of type-I IFNs or inactivated influenza virus causes a rapid decrease of PBL in both humans [7,25,26] and mice [20,27,28].

PAMPs of influenza virus, which have the ability to induce type-I IFNs, are strong candidates for the factors responsible for PBL loss. We further show that this PBL loss is completely abrogated in MyD-88 KO mice and partially in TLR7 KO mice. Among the components of influenza virus, viral ssRNA is recognized by TLR7. In formalin-inactivated virus, viral ssRNA is probably encapsulated inside the viral particles. By contrast, RNA in HA split is exposed due to the loss of capsid lipids by ether treatment, which may allow RNase in blood to degrade the viral ssRNA before it can be captured by pDCs. Nevertheless, residual undigested RNA in HA split may impact on the intensity of HA-specific Ab responses [29], considering the discrepancy in kinetics between HA split-administrated WT mice and whole virion-administrated B6.IFNα/βR KO mice. This hypothesis will be tested by further examination of PBL loss using a liposome-encapsulated HA split. Of note, partial loss of PBL in TLR7 KO mice suggests that influenza virus stimulates MyD-88-associated signaling by other PRRs. Recently, it has been shown that pDCs from TLR7 KO mice retain the potential to produce IFNα in response to whole virions [23]. Moreover, endocytosed influenza virus ssRNA could be recognized by NOD-like receptor protein 3, which results in inflammasome activation in mice [12]. Collectively, TLR7 in addition to the autocrine/paracrine IL-1β-MyD-88

mediated signal pathway may be necessary for the production of sufficient type-I IFNs necessary to induce leukocytopenia.

Viral infections [2–4] or poly (I:C) administration [21] are known to induce leukocytopenia via production of type-I IFNs, suggesting that a viral PRRs–type-I IFNs axis is responsible for the loss of PBL. However, the precise mechanisms by which type-I IFNs cause acute leukocytopenia and the different role played by each member of the type-I IFN family remain obscure. Regarding the fate of the missing leukocytes after administration of inactivated influenza virus, there are two possibilities: redistribution and cell death. Shiow et al. [22] have reported that administration of poly (I:C) or LCMV infection causes accumulation of peripheral blood lymphocytes in lymph nodes by blocking S1P receptor 1 signaling. However, we and others [28] demonstrated that S1P plays a very limited role in PBL reduction. Additionally, we detected a slight decrease of peripheral blood granulocytes, which is independent of egress from secondary lymph nodes. These discrepancies may be attributed to differences in the focus on leukocyte subsets, in the magnitude of type-I IFN production, and/or the use of different TLR ligands in each system. On the other hand, PBL rapidly undergo apoptosis in a type-I IFN dependent manner prior to the massive reduction of PBL numbers. Although the precise mechanism remains to be elucidated, it has been reported that type-I IFNs cause rapid activation of peripheral T- and B-cells [30], which may lead to activation-induced cell death [31]. Otherwise, antagonistic activity of type-I IFNs to IL-7 may affect lymphocyte survivals [14].

Several groups have reported that the type-I IFN signaling pathway is essential for proper humoral responses to the influenza vaccine [23,32,33]. However, their observations were all made at a relatively short time after immunization: within 1–2 weeks. We demonstrated that the virus-specific IgG titers in IFNα/βR KO mice were restored to control levels by 4 weeks after vaccination. Taken together, the role of type-I IFNs in influenza-specific IgG production during viral infection is evident from the previous studies, but might be overstated and limited to within a short time after vaccination with inactive whole virions.

In summary, the administration of inactivated influenza whole vaccine causes a rapid loss of PBL in an IFNα-dependent manner. The inability of HA-split vaccine to induce IFNα suggests that packaging of viral ssRNA is important for strong induction of innate immunity. The rapid apoptosis of PBL, which include circulating memory lymphocytes, may influence immune responses to other antigens, suggesting that keeping a balance between innate and acquired immunity is required for more appropriate vaccination strategies.

Appendix A. Supplementary data

Supplementary data associated with this article can be found, in the online version, at http://dx.doi.org/10.1016/j.vaccine.2013.02.016.

References

[1] Aoshi T, Koyama S, Kobiyama K, Akira S, Ishii KJ. Innate and adaptive immune responses to viral infection and vaccination. Curr Opin Virol 2011;1:226–32.

[2] Woodruff JF, Woodruff JJ. Virus-induced alterations of lymphoid tissues. I. Modification of the recirculating pool of small lymphocytes by Newcastle disease virus. Cell Immunol 1970;1:333–54.

[3] Nanan R, Chittka B, Hadam M, Kreth HW. Measles virus infection causes transient depletion of activated T cells from peripheral circulation. J Clin Virol 1999;12:201–10.

[4] Tumpey TM, Lu X, Morken T, Zaki SR, Katz JM. Depletion of lymphocytes and diminished cytokine production in mice infected with a highly virulent influenza A (H5N1) virus isolated from humans. J Virol 2000;74:6105–16.

[5] Kurokawa M, Ishida S, Asakawa S, Iwasa S, Goto N. Toxicities of influenza vaccine: peripheral leukocytic response to live and inactivated influenza viruses in mice. Jpn J Med Sci Biol 1975;28:37–52.

[6] Lewis DE, Gilbert BE, Knight V. Influenza virus infection induces functional alterations in peripheral blood lymphocytes. J Immunol 1986;137:3777–81.

[7] Faguet GB. The effect of killed influenza virus vaccine on the kinetics of normal human lymphocytes. J Infect Dis 1981;143:252–8.

[8] Schenten D, Medzhitov R. The control of adaptive immune responses by the innate immune system. Adv Immunol 2011;109:87–124.

[9] Meylan E, Tschopp J, Karin M. Intracellular pattern recognition receptors in the host response. Nature 2006;442:39–44.

[10] Diebold SS, Kaisho T, Hemmi H, Akira S, Reis e Sousa C. Innate antiviral responses by means of TLR7-mediated recognition of single-stranded RNA. Science 2004;303:1529–31.

[11] Kato H, Takeuchi O, Sato S, Yoneyama M, Yamamoto M, Matsui K, et al. Differential roles of MDA5 and RIG-I helicases in the recognition of RNA viruses. Nature 2006;441:101–5.

[12] Ichinohe T, Lee HK, Ogura Y, Flavell R, Iwasaki A. Inflammasome recognition of influenza virus is essential for adaptive immune responses. J Exp Med 2009;206:79–87.

[13] Pestka S, Krause CD, Walter MR. Interferons, interferon-like cytokines, and their receptors. Immunol Rev 2004;202:8–32.

[14] Bogdan C, Mattner J, Schleicher U. The role of type I interferons in non-viral infections. Immunol Rev 2004;202:33–48.

[15] Le Bon A, Etchart N, Rossmann C, Ashton M, Hou S, Gewert D, et al. Cross-priming of CD8+ T cells stimulated by virus-induced type I interferon. Nat Immunol 2003;4:1009–15.

[16] Jego G, Palucka AK, Blanck JP, Chalouni C, Pascual V, Banchereau J. Plasmacytoid dendritic cells induce plasma cell differentiation through type I interferon and interleukin 6. Immunity 2003;19:225–34.

[17] Reimer CB, Baker RS, Newlin TE, Havens ML. Influenza virus purification with the zonal ultracentrifuge. Science 1966;152:1379–81.

[18] Davenport FM, Hennessy AV, Brandon FM, Webster RG, Barrett Jr CD, Lease GO. Comparisons of serologic and febrile responses in humans to vaccination with influenza A viruses or their hemagglutinins. J Lab Clin Med 1964;63:5–13.

[19] Ato M, Nakano H, Kakiuchi T, Kaye PM. Localization of marginal zone macrophages is regulated by C-C chemokine ligands 21/19. J Immunol 2004;173:4815–20.

[20] Takahashi Y, Inamine A, Hashimoto S, Haraguchi S, Yoshioka E, Kojima N, et al. Novel role of the Ras cascade in memory B cell response. Immunity 2005;23:127–38.

[21] Korngold R, Blank KJ, Murasko DM. Effect of interferon on thoracic duct lymphocyte output: induction with either poly I:poly C or vaccinia virus. J Immunol 1983;130:2236–40.

[22] Shiow LR, Rosen DB, Brdicková N, Xu Y, An J, Lanier LL, et al. CD69 acts downstream of interferon-alpha/beta to inhibit S1P1 and lymphocyte egress from lymphoid organs. Nature 2006;440:540–4.

[23] Geeraedts F, Goutagny N, Hornung V, Severa M, de Haan A, Pool J, et al. Superior immunogenicity of inactivated whole virus H5N1 influenza vaccine is primarily controlled by Toll-like receptor signalling. PLoS Pathog 2008;4:e1000138.

[24] Koyama S, Aoshi T, Tanimoto T, Kumagai Y, Kobiyama K, Tougan T, et al. Plasmacytoid dendritic cells delineate immunogenicity of influenza vaccine subtypes. Sci Transl Med 2010;2:25ra24.

[25] Schattner A, Meshorer A, Wallach D. Involvement of interferon in virus-induced lymphopenia. Cell Immunol 1983;79:11–25.

[26] Gillespie JH, Scott FW, Geissinger CM, Czarniecki CW, Scialli VT. Levels of interferon in blood serum and toxicity studies of bacteria-derived bovine alpha$_i$1 interferon in dairy calves. J Clin Microbiol 1986;24:240–4.

[27] Degré M. Influence of exogenous interferon on the peripheral white blood cell count in mice. Int J Cancer 1974;14:699–703.

[28] Kamphuis E, Junt T, Waibler Z, Forster R, Kalinke U. Type I interferons directly regulate lymphocyte recirculation and cause transient blood lymphopenia. Blood 2006;108:3253–61.

[29] Jeisy-Scott V, Kim JH, Davis WG, Cao W, Katz JM, Sambhara S. TLR7 recognition is dispensable for influenza virus A infection, but important for the induction of hemagglutinin-specific antibodies in response to the 2009 pandemic split vaccine in mice. J Virol 2012;86:10988–98.

[30] Alsharifi M, Lobigs M, Regner M, Lee E, Koskinen A, Müllbacher A. Type I interferons trigger systemic, partial lymphocyte activation in response to viral infection. J Immunol 2005;175:4635–40.

[31] Manna SK, Mukhopadhyay A, Aggarwal BB. IFN-alpha suppresses activation of nuclear transcription factors NF-kappa B and activator protein 1 and potentiates TNF-induced apoptosis. J Immunol 2000;165:4927–34.

[32] Proietti E, Bracci L, Puzelli S, Di Pucchio T, Sestili P, De Vincenzi E, et al. Type I. IFN as a natural adjuvant for a protective immune response: lessons from the influenza vaccine model. J Immunol 2002;169:375–83.

[33] Coro ES, Chang WL, Baumgarth N. Type I. IFN receptor signals directly stimulate local B cells early following influenza virus infection. J Immunol 2006;176:4343–51.

Replication of Hepatitis C Virus Genotype 3a in Cultured Cells

MOHSAN SAEED,[1] CLAIRE GONDEAU,[2] SUSU HMWE,[1] HIROSHI YOKOKAWA,[1,3] TOMOKO DATE,[1] TETSURO SUZUKI,[1] TAKANOBU KATO,[1] PATRICK MAUREL,[2] and TAKAJI WAKITA[1]

[1]Department of Virology II, National Institute of Infectious Diseases, Tokyo, Japan; [2]Inserm U1040, Biotherapy Research Institute, Montpellier, France; and [3]Pharmaceutical Research Laboratories, Toray Industries, Inc., Kanagawa, Japan

---

Hepatitis C virus (HCV) genotype 3a is widespread worldwide, but no replication system exists for its study. We describe a subgenomic replicon system for HCV genotype 3a. We determined the consensus sequence of an HCV genome isolated from a patient, and constructed a subgenomic replicon using this clone. The replicon was transfected into HuH-7 cells and RNA replication was confirmed. We identified cell culture-adaptive mutations that increased colony formation multiple-fold. We have therefore established a genotype 3a replicon system that can be used to study this HCV genotype.

Keywords: Virology; Experimental Model; HCVGT3; In Vitro Culture System.

Hepatitis C virus (HCV) infection leads to chronic infection and advanced liver diseases in most infected adults.[1] Of the 6 major HCV genotypes, genotypes 1 and 2 are the most prevalent in North America, Europe, and Japan,[2,3] and are the most highly studied. However, other genotypes display specific characteristics. For example, genotype 3a infection can result in hepatic steatosis[4] and telaprevir and boceprevir are less effective against genotype 3a.[5] Therefore, the pathogenesis and inhibitor sensitivity of all HCV genotypes should be studied. Although HCV subgenomic replicons are useful for understanding viral/host factors involved in HCV replication and inhibitor sensitivity, only HCV replicons for genotypes 1a, 1b, and 2a have been established.[6–9] Here, we report on the robust genotype 3a replication system.

An almost complete HCV genome was recovered from the serum of a patient with post-transplantation recurrent HCV infection. This serum exhibited higher infectivity than other tested sera toward primary human hepatocytes (Supplementary Figure 1A). The isolate, named S310, contained the following structural elements: a 5'UTR (nt 1-339), an open reading frame encoding 3021 aa (nt 340-9402), and a 3'UTR (nt 9403-9654). Only the last 44 nt of the X-region (nt 9611-9654) could not be recovered. Two major virus populations were found; S310/A contained Ala, Thr, Thr, and Ile, and S310/B contained Thr, Ala, Ala, and Thr, at the 7th, 151st, 431st, and 472nd aa of the NS3 protein, respectively. S310 was clustered into genotype 3a by phylogenetic analysis (Supplementary Figure 1B). The complexity of the virus quasispecies in the serum was analyzed by sequencing the hypervariable region. Identical amino acid sequences in all 10 hypervariable region clones indicated a very low degree of diversity. The hypervariable region sequence of the JFH-1 strain also exhibited monoclonality,[10] which can be important for efficient replication in cultured cells.

Subgenomic replicons SGR-S310/A and SGR-S310/B were constructed and their replication efficiency was evaluated by G418-resistant colony-formation assay. After 3 weeks, a small number of colonies were visible for both replicons (Figure 1A). Because more colonies were observed in SGR-S310/A than in SGR-S310/B, we focused on SGR-S310/A (henceforth called SGR-S310). Ten cell colonies of SGR-S310 were isolated and analyzed for HCV replication. The mean RNA titer was $9.1 \times 10^7 \pm 4.6 \times 10^7$ copies/μg total RNA (Figure 1B). HCV RNA (approximately 8 kb) was detected by Northern blotting (Supplementary Figure 2A). Viral proteins in the replicon cells were detected by immunofluorescence and Western blotting (Supplementary Figure 2B and 2C). To determine whether the G418 resistance of the cells was transmissible by cellular RNA transfection, we electroporated total cellular RNA isolated from 4 replicon clones into naïve HuH-7 cells. Multiple G418-resistant colonies appeared after transfection of the RNA isolated from the replicon clones (Supplementary Figure 3A), but not from the naïve HuH-7 cells. These results indicate that the replicon RNA in the parental colonies could replicate in naïve cells. Thus, the G418-resistant colonies that were isolated from cells electroporated with SGR-S310 synthetic RNA contained replicating viral RNA.

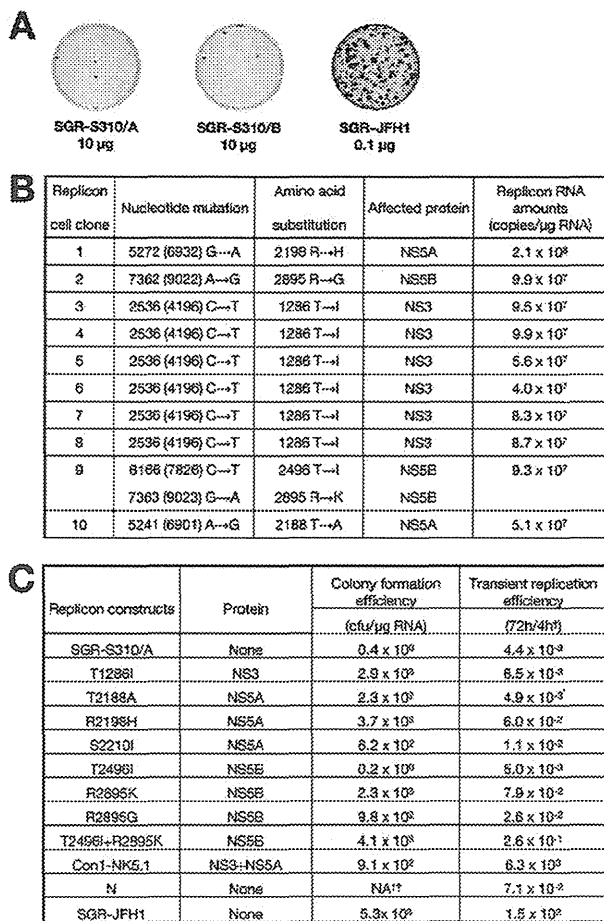Replicating genomes have been shown to accumulate cell culture adaptive mutations, which increase their replication potential. To examine whether SGR-S310 acquired mutations, the complete HCV sequences from 10 replicon clones were sequenced. At least one nonsynonymous mutation was detected in the NS3-NS5B region of each replicon clone (Figure 1B). The following mutations were identified: T1286I in the NS3 helicase (6 of 10

A

SGR-S310/A 10 µg   SGR-S310/B 10 µg   SGR-JFH1 0.1 µg

B

Replicon cell clone	Nucleotide mutation	Amino acid substitution	Affected protein	Replicon RNA amounts (copies/µg RNA)
1	5272 (6932) G→A	2198 R→H	NS5A	2.1×10^8
2	7362 (9022) A→G	2895 R→G	NS5B	9.9×10^7
3	2536 (4196) C→T	1286 T→I	NS3	9.5×10^7
4	2536 (4196) C→T	1286 T→I	NS3	9.9×10^7
5	2536 (4196) C→T	1286 T→I	NS3	6.6×10^7
6	2536 (4196) C→T	1286 T→I	NS3	4.0×10^7
7	2536 (4196) C→T	1286 T→I	NS3	8.3×10^7
8	2536 (4196) C→T	1286 T→I	NS3	8.7×10^7
9	8166 (7826) C→T	2496 T→I	NS5B	9.3×10^7
	7363 (9023) G→A	2895 R→K	NS5B	
10	5241 (6901) A→G	2188 T→A	NS5A	5.1×10^7

C

Replicon constructs	Protein	Colony formation efficiency (cfu/µg RNA)	Transient replication efficiency (72h/4h)
SGR-S310/A	None	0.4×10^0	4.4×10^{-3}
T1286I	NS3	2.9×10^2	6.5×10^{-3}
T2188A	NS5A	2.3×10^3	4.9×10^{-3}
R2198H	NS5A	3.7×10^3	6.0×10^{-2}
S2210I	NS5A	6.2×10^2	1.1×10^{-3}
T2496I	NS5B	0.2×10^0	5.0×10^{-3}
R2895K	NS5B	2.3×10^2	7.9×10^{-2}
R2895G	NS5B	9.8×10^3	2.6×10^{-2}
T2496I+R2895K	NS5B	4.1×10^3	2.6×10^{-1}
Con1-NK5.1	NS3-NS5A	9.1×10^2	6.3×10^3
N	None	NA††	7.1×10^{-2}
SGR-JFH1	None	5.3×10^2	1.5×10^2

Figure 1. S310 subgenomic replicon analysis. (A) Three million HuH-7 cells were electroporated with 10 µg RNA from SGR-S310/A or SGR-S310/B or 0.1 µg RNA from SGR-JFH1. G418-selected colonies were fixed and stained after 3 weeks. (B) Non-synonymous mutations identified in the replicon genomes and HCV RNA titers in the replicon clones. Nucleotide positions within the S310 subgenomic replicon and within the full-length S310 genome (in parentheses) are given. (C) Replication potential of the adaptive mutants as determined by the colony-formation assay using Neo-replicons and by the transient replication assay using Fluc-replicons. †72 h/4 h, transient replication efficiency was determined as a ratio of luciferase activity in the transfected cells between 72 h and 4 h post transfection. ††NA, not available.

clones); T2188A or R2198H in NS5A (2 clones); an R2895G substitution in NS5B (1 clone); and T2496I in NS5A plus R2895K in NS5B (1 clone). These mutations and the S2210I mutation (corresponding to S2204I in genotype 1 replicon)[7,8] were introduced, individually or in combination, into the parental SGR-S310 and the colony-formation efficiencies of the mutant replicons were tested. All mutations, except T2496I, increased the colony formation, indicating an adaptive phenotype (Figure 1C, Supplementary Figure 3B). Transient replication efficiency was also tested using firefly luciferase reporter replicons. SGR-S310/Luc did not replicate in Huh-7.5.1 cells, whereas the adaptive mutants displayed varying degrees of replication (Figure 1C, Supplementary Figure 3C). Adaptive mutations T2496I and R2895K, when combined to-

gether, most efficiently enhanced the colony formation as well as transient replication (Figure 1C). Interestingly, T1286I and R2895G found in our study correspond to the Con1 adaptive mutations T1280I and R2884G, respectively.[11,12] T2188A or R2198H in NS5A were identified in 2 replicon clones and are located close to S2210I. Indeed, S2210I also enhanced SGR-S310 replication, suggesting that this region might be important for HCV replication. S310 replicons with adaptive mutations were compared with genotype 1b (Con1 and N) and 2a (JFH-1) replicons. Colony-formation efficiencies of most S310 adaptive replicons were at levels comparable with Con1 and JFH-1 (Figure 1C, Supplementary Figure 3B). In contrast, S310 adaptive replicons replicated less efficiently than Con1-NK5.1 and JFH-1 replicons in transient replication assays. However, genotype 1b N replicon replicated at a level similar to some S310 adaptive replicons (Figure 1C, Supplementary Figure 3C). Future studies will dissect the detailed mechanisms that underlie the effects of these mutations.

Successful generation of a genotype 3a replicon provided a unique opportunity to compare the susceptibility of genotype 3a (SGR-S310), 1b (Con1[13]), and 2a (JFH-1/4-1[13]) replicons to HCV inhibitors. Interferon-alfa dose-dependently decreased the replication of all tested genotypes (Figure 2A), whereas a protease inhibitor, BILN-2061, was more effective against replicons from genotypes 1b and 2a than 3a (Figure 2B). The non-nucleoside polymerase inhibitor JTK-109 was more potent against genotype 1b and 3a (Figure 2C). However, the nucleoside polymerase inhibitor, PSI-6130, equally inhibited all genotypes (Figure 2D).

In conclusion, we established a subgenomic replicon for genotype 3a, which should be useful for understanding the specific characteristics of this genotype and for the screening of antiviral chemicals that are effective against this genotype. Construction of a full-length infectious S310 clone is in progress.

Supplementary Material

Note: To access the supplementary material accompanying this article, visit the online version of *Gastroenterology* at www.gastrojournal.org, and at http://dx.doi.org/10.1053/j.gastro.2012.09.017.

References

1. Di Bisceglie AM. Hepatology 1997;26(Suppl):34S–38S.
2. Lauer GM, et al. N Engl J Med 2001;345:41–52.
3. Ohno T, et al. J Clin Microbiol 1997;35:201–207.
4. Hui JM, et al. J Gastroenterol Hepatol 2002;17:873–881.
5. Gottwein, JM et al. Gastroenterology 2011;141:1067–1079.
6. Lohmann, V et al. Science 1999;285:110–113.
7. Blight KJ, et al. Science 2000;290:1972–1974.
8. Blight KJ, et al. J Virol 2003;77:3181–3190.
9. Kato T, et al. Gastroenterology 2003;125:1808–1817.
10. Kato T, et al. J Med Virol 2001;64:334–339.
11. Krieger N, et al. J Virol 2001;75:4614–4624.
12. Lohmann V, et al. J Virol 2001;75:1437–1449.